





# The *SYNGAP1* 3' UTR Variant in ALS Patients Causes Aberrant *SYNGAP1* Splicing and Dendritic Spine Loss by Recruiting HNRNPK

Satoshi Yokoi,<sup>1</sup>  Takuji Ito,<sup>2,3</sup> Kentaro Sahashi,<sup>1</sup>  Masahiro Nakatochi,<sup>4</sup> Ryoichi Nakamura,<sup>1,2</sup> Genki Tohno,<sup>5</sup> Yusuke Fujioka,<sup>1</sup> Shinsuke Ishigaki,<sup>1,6</sup> Tsuyoshi Udagawa,<sup>7</sup> Yuishin Izumi,<sup>8</sup> Mitsuya Morita,<sup>9</sup> Osamu Kano,<sup>10</sup> Masaya Oda,<sup>11</sup> Takefumi Sone,<sup>12</sup>  Hideyuki Okano,<sup>12</sup> Naoki Atsuta,<sup>1,2</sup> Masahisa Katsuno,<sup>1</sup>  Yohei Okada,<sup>2,3</sup> and Gen Sobue<sup>6,13</sup>

<sup>1</sup>Department of Neurology, Nagoya University Graduate School of Medicine, Nagoya 466-8550, Japan, <sup>2</sup>Department of Neurology, Aichi Medical University School of Medicine, Aichi 480-1195, Japan, <sup>3</sup>Department of Neural iPSC Research, Institute for Medical Science of Aging, Aichi Medical University, Aichi 480-1195, Japan, <sup>4</sup>Public Health Informatics Unit, Department of Integrated Health Sciences, Nagoya University Graduate School of Medicine, Nagoya 461-8673, Japan, <sup>5</sup>Division of ALS Research, Aichi Medical University, Aichi 480-1195, Japan, <sup>6</sup>Research Division of Dementia and Neurodegenerative Disease, Nagoya University Graduate School of Medicine, Nagoya 466-8550, Japan, <sup>7</sup>Graduate School of Pharmaceutical Sciences, Nagoya City University, Nagoya 467-8603, Japan, <sup>8</sup>Department of Neurology, Institute of Biomedical Sciences, Tokushima University Graduate School, Tokushima 770-8503, Japan, <sup>9</sup>Division of Neurology, Department of Internal Medicine, Jichi Medical University, Shimotsuke 329-0498, Japan, <sup>10</sup>Department of Neurology, Toho University Faculty of Medicine, Tokyo 143-8540, Japan, <sup>11</sup>Department of Neurology, Vihara Hananosato Hospital, Miyoshi 728-0001, Japan, <sup>12</sup>Department of Physiology, Keio University School of Medicine, Tokyo 160-0016, Japan, and <sup>13</sup>Aichi Medical University, Aichi 480-1195, Japan

Fused in sarcoma (FUS) is a pathogenic RNA-binding protein in amyotrophic lateral sclerosis (ALS). We previously reported that FUS stabilizes Synaptic Ras-GTPase activating protein 1 (*Syngap1*) mRNA at its 3' untranslated region (UTR) and maintains spine maturation. To elucidate the pathologic roles of this mechanism in ALS patients, we identified the *SYNGAP1* 3'UTR variant rs149438267 in seven (four males and three females) out of 807 ALS patients at the FUS binding site from a multicenter cohort in Japan. Human-induced pluripotent stem cell (hiPSC)-derived motor neurons with the *SYNGAP1* variant showed aberrant splicing, increased isoform  $\alpha 1$  levels, and decreased isoform  $\gamma$  levels, which caused dendritic spine loss. Moreover, the *SYNGAP1* variant excessively recruited FUS and heterogeneous nuclear ribonucleoprotein K (HNRNPK), and antisense oligonucleotides (ASOs) blocking HNRNPK altered aberrant splicing and ameliorated dendritic spine loss. These data suggest that excessive recruitment of RNA-binding proteins, especially HNRNPK, as well as changes in *SYNGAP1* isoforms, are crucial for spine formation in motor neurons.

**Key words:** amyotrophic lateral sclerosis; antisense oligonucleotides; dendritic spine; hnRNPK; iPSC-derived motor neuron; SYNGAP1

Received Feb. 25, 2022; revised Aug. 28, 2022; accepted Oct. 6, 2022.

Author contributions: G.S. and S.Y. designed research; S.Y., T.I., K.S., M.N., R.N., Y.F., N.A., and Y.O. performed research; G.T., S.I., Y.I., M.M., O.K., M.O., T.S., H.O., N.A., and M.K. contributed unpublished reagents/analytic tools; S.Y., T.I., K.S., M.N., R.N., T.U., N.A., and Y.O. analyzed data; S.Y. wrote the first draft of the paper; G.S., S.Y., K.S., Y.F., S.I., T.U., Y.I., M.M., O.K., M.O., T.S., H.O., N.A., and M.K. edited the paper; T.I., K.S., M.N., R.N., and Y.O. wrote the paper.

This work was supported by Japan Agency for Medical Research and Development (AMED) Grants JP22ek0109434, JP19ek0109243, JP22bm0804003, JP22bm0804020, 22ak0101111, 22ek0109492, and 24wm0425009; Japan Society for the Promotion of Science (JSPS) KAKENHI Grants JP20K16489, JP19H03576, and JP22H02988; the Hori Sciences & Arts Foundation; and the Japan and Kanoe Foundation for the promotion of medical science, Japan. This work is partially supported by Nagoya University Research Fund. We thank Hiroyuki Mizuguchi for the kind gift of plasmids, Shinya Yamanaka

for the kind gift of human iPSCs (201B7), and Kentaro Taki for technical support with LC/MS/MS in the laboratory of the Division for Medical Research Engineering, Nagoya University Graduate School of Medicine.

The authors declare no competing financial interests.

Correspondence should be addressed to Yohei Okada at yohei@aichi-med-u.ac.jp or Gen Sobue at sobueg@aichi-med-u.ac.jp.

<https://doi.org/10.1523/JNEUROSCI.0455-22.2022>

Copyright © 2022 Yokoi et al.

This is an open-access article distributed under the terms of the Creative Commons Attribution 4.0 International license, which permits unrestricted use, distribution and reproduction in any medium provided that the original work is properly attributed.

### Significance Statement

It is not yet known which RNAs cause the pathogenesis of amyotrophic lateral sclerosis (ALS). We previously reported that Fused in sarcoma (FUS), a pathogenic RNA-binding protein in ALS, stabilizes synaptic Ras-GTPase activating protein 1 (*Syngap1*) mRNA at its 3' untranslated region (UTR) and maintains dendritic spine maturation. To elucidate whether this mechanism is crucial for ALS, we identified the *SYNGAP1* 3'UTR variant rs149438267 at the FUS binding site. Human-induced pluripotent stem cell (hiPSC)-derived motor neurons with the *SYNGAP1* variant showed aberrant splicing, which caused dendritic spine loss along with excessive recruitment of FUS and heterogeneous nuclear ribonucleoprotein K (HNRNPK). Our findings that dendritic spine loss is because of excess recruitment of RNA-binding proteins provide a basis for the future exploration of ALS-related RNA-binding proteins.

### Introduction

Fused in sarcoma (*FUS*) is one of the major causative genes for amyotrophic lateral sclerosis (ALS) and frontotemporal lobar degeneration (FTLD; Kwiatkowski et al., 2009; Neumann et al., 2009). The key pathologic findings of ALS-FUS or ALS/FTLD are the cytosolic mislocalization and aggregate formations of FUS (Neumann et al., 2009; Mackenzie et al., 2011), suggesting either the gain-of-toxic function (Sharma et al., 2016; López-Erauskin et al., 2018) or loss-of-function (Ishigaki and Sobue, 2018; Humphrey et al., 2020) of FUS. Abnormal liquid–liquid phase separation of FUS is also reported to be involved in the potential pathogenesis of FUS aggregation (Hofweber et al., 2018; Niaki et al., 2020).

FUS is an RNA-binding protein that is involved in various RNA metabolisms, including alternative splicing (Ishigaki et al., 2012; Lagier-Tourenne et al., 2012), mRNA stability (Kapeli et al., 2016), transcription (Tan and Manley, 2010; Masuda et al., 2015), mRNA transport (Fujii et al., 2005), and translation (Yasuda et al., 2013; Kamelgarn et al., 2018). FUS binds to the 3' untranslated region (UTR) of its target mRNAs (Ishigaki et al., 2012; Lagier-Tourenne et al., 2012; Nakaya et al., 2013) and post-transcriptionally regulates mRNA expression (Udagawa et al., 2015; Yokoi et al., 2017; Akiyama et al., 2019; Garone et al., 2020). While aberrant RNA metabolism of FUS has been suggested to correlate with the pathogenesis of ALS/FTLD, it is still not clear which specific RNA pathway might directly cause ALS/FTLD.

Synaptic dysfunction is considered an initial pathologic change in ALS and various neurodegenerative diseases (Hermes and Dorostkar, 2016; Henstridge et al., 2018). Importantly, FUS is known to be involved in synaptic function (Fujii et al., 2005; Qiu et al., 2014; Deshpande et al., 2019). We have investigated the relationship between FUS and synaptic function and found that FUS regulates the mRNA stability of Glutamate ionotropic receptor AMPA type subunit 1 (*Gria1*; Udagawa et al., 2015) and Synaptic Ras-GTPase activating protein 1 (*Syngap1*; Yokoi et al., 2017) at their 3' UTR, thus maintaining spine morphology and cognitive function. *SYNGAP1* is a pathogenic gene for intellectual disability including mental retardation, epilepsy, and autism spectrum disorders (Mignot et al., 2016), and *SYNGAP1* is a major protein located at the postsynaptic density and negatively regulates the Ras/Rap pathway (Kim et al., 1998; Jayabalan and Clement, 2016; Walkup et al., 2016). *Syngap1* knock-out mice exhibit an increased number of mature spines (Kim et al., 2003; Clement et al., 2012). *SYNGAP1* has four isoforms that exert different synaptic functions and are defined by their C terminals:  $\alpha 1$ ,  $\alpha 2$ ,  $\beta$ , and  $\gamma$  (McMahon et al., 2012; Araki et al., 2020). For instance, the isoform  $\alpha 1$  decreases synaptic strength, while  $\alpha 2$  increases synaptic strength (McMahon et al.,

2012). We previously reported that FUS specifically binds to the long 3'UTR of *Syngap1*, which is mainly connected to the *Syngap1* isoform  $\alpha 2$  mRNA involved in strengthening synaptic function (Yokoi et al., 2017). Although these findings indicate that FUS-mediated *Syngap1* mRNA regulation is important for spine maturation in mice, its involvement in the pathogenesis of ALS/FTLD has never been described.

Therefore, we explored the whole exome sequencing data of the Japanese Consortium for Amyotrophic Lateral Sclerosis Research (JaCALS; a multicenter ALS cohort in Japan; Hayashi et al., 2020; Nakamura et al., 2021). We searched for a causative variant in the *SYNGAP1* 3'UTR binding site of FUS that might induce the aberrant binding properties of FUS, which cause aberrant *SYNGAP1* mRNA metabolism and synaptic dysfunction. As the *SYNGAP1* 3'UTR binding site of FUS in humans is different from that in mice (Nakaya et al., 2013), analyses using human-derived samples are mandatory for investigating the pathogenesis of the variant. Thus, the isogenic model of human-induced pluripotent stem cell (iPSC)-derived motor neurons were used to validate the pathogenic mechanism of the novel *SYNGAP1* variant in human ALS patients.

### Materials and Methods

#### Study approval

The experiments using information and material related to patients with the *SYNGAP1* variant were approved by the ethics committee of Nagoya University Graduate School of Medicine (2004-0281). All the experimental procedures for the production and use of iPSCs were approved by the ethics committee of the Aichi Medical University School of Medicine (approval number 14-004, 2020-213).

#### Genetic analysis

We performed whole exome sequencing in 807 patients with sporadic ALS and in 191 normal controls who had previously participated in the Japanese Consortium for Amyotrophic Lateral Sclerosis Research (JaCALS), which consists of 32 neurologic facilities. The details of JaCALS have been described elsewhere (Hayashi et al., 2020).

Genomic DNA was extracted from peripheral blood leukocytes. The exomes of patients with sporadic ALS were captured with the SureSelect Human All Exon V5+UTR or V6+UTR (Agilent Technologies). The libraries were indexed, pooled, and sequenced on an Illumina HiSeq 2000 Sequencer (paired-end, 100 base reads). The reads were aligned to a human reference genome (UCSC hg19) using BWA 0.6.2. The Picard tools 1.73 software was used to remove duplicate reads. Variants and insertions/deletions were identified with GATK 1.6–13 and filtered to the coordinates with variant quality score recalibration. NM\_006772 (RefSeq) was referred to identify the 3'UTR region in the *SYNGAP1* gene, and variants within the FUS binding sites of the *SYNGAP1* 3'UTR were then selected. According to the CLIP-seq data of FUS in the human brain (Nakaya et al., 2013), the FUS binding sites were defined as those identified in multiple patients. The *SYNGAP1* 3'UTR variants (rs149438267) found in four males and three females were validated

using Sanger sequencing. The sequence variants were validated by sequencing in both directions. There were no known pathogenic mutations for ALS in patients with the *SYNGAP1* 3'UTR variant. The sequencing details have been previously described (Nakamura et al., 2021).

#### *hiPSC culture and differentiation in vitro*

The experiments were performed as described previously (Shimojo et al., 2015; Onodera et al., 2020; Okada et al., 2021). 201B7 cells (a gift from Shinya Yamanaka) were maintained on mitomycin-C-treated murine fibroblast STO cell line transformed with neomycin resistance and murine LIF genes (SNL) feeder cells in 0.1% gelatin-coated tissue culture dishes in human embryonic stem cell (hESC) medium, and were used to induce motor neurons. For differentiation, the SNL feeder cells were first removed. Then, hiPSC colonies were detached using a dissociation solution containing 0.25% trypsin, 100  $\mu$ g/ml Collagenase IV, 1 mM CaCl<sub>2</sub>, and 20% knock-out serum replacement (KSR) medium, and were cultured in suspension in bacteriologic dishes in standard hESC medium without basic fibroblast growth factor for 1–2 h in gelatin-coated dishes. On day 1, the medium was changed to human embryoid body (hEB) medium containing DMEM/F-12, 5% KSR, 2 mM L-glutamine, 1% non-essential amino acids solution (NEAA) and 0.1 mM 2-mercaptoethanol with 300 nM LDN-193189, 3  $\mu$ M SB 431542, and 3  $\mu$ M CHIR 99021. On day 2, the medium was changed to fresh hEB medium containing 300 nM LDN-193189, 3  $\mu$ M SB431542, 3  $\mu$ M CHIR99021, and 1  $\mu$ M retinoic acid. On days 4–14, hEBs were cultured in hEB medium containing 1  $\mu$ M retinoic acid and 1  $\mu$ M purmorphamine; the medium was changed every 2–3 d. On day 14, hEBs were dissociated into single cells using TrypLE Select. The dissociated cells were plated on dishes coated with growth factor reduced Matrigel at a density of  $1 \times 10^5$  cells/cm<sup>2</sup>, and were cultured in motor neuron medium consisting of KBM Neural Stem Cell medium supplemented with 2% B27 supplement, 1% CultureOne supplement, 1% NEAA, 50 nM retinoic acid, 500 nM purmorphamine, 10  $\mu$ M cyclic AMP, 10 ng/ml recombinant brain-derived neurotrophic factor (BDNF), 10 ng/ml recombinant glial cell line derived neurotrophic factor (GDNF), 10 ng/ml recombinant human insulin-like growth factor-1 (IGF-1), and 200 ng/ml L-ascorbic acid for up to four weeks. Half of the medium was changed every 2–3 d.

#### *Scarless genome editing in iPSCs*

The donor plasmid (Yoshimatsu et al., 2019) was generated for scarless genome editing. The TTAA site in *SYNGAP1* 3'UTR was selected as the center of the 5' and 3' arm. The primers for cloning the *SYNGAP1* 3'UTR sequence are listed in Table 1. The plasmids pENTR2-L3-PBL-R1 (for the 5' arm) and pENTR2-R2-PBR-L4 (for the 3' arm) were linearized by HpaI and ligated with the cloned sequences by Gibson's assembly. To construct the donor plasmid, Multisite Gateway LR cloning was performed with the generated vectors with the arms as follows: pENTR-L1-PGK-PuroTK-L2 and pUC-DEST-R3R4. To generate single-guide RNAs (sgRNAs) targeting the *SYNGAP1* variant, the Guide-it sgRNA In Vitro Transcription kit (Takara) was used according to the manufacturer's instructions. We generated sgRNA targeting AAGAGAGGGCAGCACCCCAATGG to generate the homozygous mutation and CCCCTTTTCCTTCCCATTGGGG to generate the heterozygous mutation. Y-27632 (10  $\mu$ M) and valproic acid (10  $\mu$ M) were added to iPSC culture medium 24 h before electroporation. On day 1, iPSCs were dissociated from SNL feeder cells into single cells using TrypLE Select (Thermo Fisher Scientific). Guide-it Recombinant Cas9 (Takara) was used for the Cas9-sgRNA ribonucleoprotein (RNP) complex. RNP, donor plasmid, and Rad51-expressing plasmid (a kind gift from Mizuguchi; Takayama et al., 2017) were introduced into iPSCs by electroporation according to the manufacturer's instructions. The iPSCs were then plated onto three 10 cm dishes in twofold dilution. On days 3 and 4, puromycin (10  $\mu$ M) was added for the selection process. After two weeks, single colonies were picked, and the *piggyBac* cassette insertion was screened by Sanger sequences. For *piggyBac* transposition, the pCAGS-PBx plasmid was introduced into the cell lines with optimal *piggyBac* cassette insertion by electroporation. Next, ganciclovir (2.5  $\mu$ g/ml) was added on days 2–4 after electroporation. After two weeks, single colonies were picked

and screened by Sanger sequences and restriction enzyme treatment (MslI). The karyotypes were confirmed to be normal in all the edited cell lines (data not shown).

#### *Antisense oligonucleotide (ASO) treatment*

For this treatment, 2'-O-methyl RNA/DNA oligonucleotides with a phosphorothioate backbone were generated by Integrate DNA Technologies (IDT). Two thirds of the nucleotides were modified in 2'-O-methyl RNA. Next, the ASOs (50 nM) were added directly to the culture medium without any transfection reagents on day 14 after plating the motor neuron cultures.

#### *Biotinylated RNA pull-down assay*

To assess the interaction of *SYNGAP1* mRNA 3'UTR with endogenous RNA-binding proteins, a biotinylated RNA pull-down assay was performed as described in previous studies (Udagawa et al., 2015; Yokoi et al., 2017). The *SYNGAP1* 3'UTR sequence was amplified from the plasmids produced in the 3' rapid amplification of cDNA ends (RACE) of wild-type (WT) iPSC-derived motor neurons. The mutation was introduced using the PrimeSTAR Mutagenesis Basal kit (Takara), according to the manufacturer's instructions. DNA templates were amplified using RT-PCR and the primers 5'-TAATACGACTCACTATAGGGCCCCACCCAGCATCAGAGACC-3' and 5'-GTCCCTGGGGTCAAAGAGA-3', and were purified using a PCR purification kit (QIAGEN) as a template for *in vitro* transcription. T7 RNA polymerase (Takara) with biotin RNA labeling mix (Roche) was used for *in vitro* transcription according to the manufacturer's instructions. The lysate containing 300  $\mu$ g of the proteins from the motor neuron cultures was incubated with 3  $\mu$ g biotinylated RNA for 1 h at room temperature; then, streptavidin Dynabeads (Invitrogen) were added. After 1 h of incubation at 4°C, the beads were washed with Brain IP buffer three times, boiled with 4 $\times$  NuPAGE LDS-PAGE sample buffer (Novex) containing  $\beta$ -mercaptoethanol for 5 min at 95°C, and analyzed with Western blotting. The band intensities of the input and pull-down were quantified.

#### *Liquid chromatography-mass spectrometry (LC-MS/MS) analysis*

For the LC-MS/MS analysis, proteins from the pull-down assay were stained with the Silver Stain kit (Invitrogen), and the bands of interest were excised and destained according to the manufacturer's instructions. After reduction and alkylation, the proteins were digested by trypsin for 16 h at 37°C. The peptides were analyzed using LC-MS with an Orbitrap Fusion mass spectrometer (Thermo Fisher Scientific) coupled to an UltiMate3000 RSLCnano LC system (Dionex Co) using a nano HPLC capillary column [150 mm  $\times$  75  $\mu$ m inner diameter (i.d.); Nikkyo Technos Co] via a nanoelectrospray ion source. Reversed-phase chromatography was performed with a linear gradient (0 min, 5% B; 100 min, 40% B) of solvent A (2% acetonitrile with 0.1% formic acid) and solvent B (95% acetonitrile with 0.1% formic acid) at an estimated flow rate of 300 nl/min. A precursor ion scan was conducted using a 400–1600 mass-to-charge ratio (m/z) before MS/MS analysis. Tandem MS was performed by isolation at 0.8 Th with the quadrupole, HCD fragmentation with a normalized collision energy of 30%, and rapid scan MS analysis in the ion trap. Only those precursors with a charge state of 2–6 were sampled for MS2. The dynamic exclusion duration was set to 15 s with a tolerance of 10 ppm. The instrument was run in top-speed mode with 3-s cycles. The raw data were processed using Proteome Discoverer 1.4 (Thermo Fisher Scientific) in conjunction with the MASCOT search engine, version 2.7.0 (Matrix Science), for protein identification. Peptides and proteins were identified against the human protein database in UniProt (release 2021\_01), with a precursor mass tolerance of 10 ppm and a fragment ion mass tolerance of 0.8 Da. The fixed modification was set to cysteine carbamidomethylation, and the variable modifications were set to methionine oxidation. Two missed cleavages by trypsin were allowed. LC/MS/MS data of pull-down assay in Extended Data Table 4-1 have been deposited at PRIDE and are publicly available as of the date of publication (project accession: PXD026586; project DOI: 10.6019/PXD026586).

**Table 1. List of primers, oligonucleotides, and antibodies used in this study**

Primers	Source	
3' RACE F primer GATTACGCCAAGCTTGCAGGCTGCTCCAGGAAGAACAA	This study	
3' UTR DNA F primer: TCTGGTTTCTGGTGTGACA	This study	
3' UTR DNA R primer: AACGAAAAGGATGAAGGGG	This study	
3' UTR F primer: TGGAAGAGTATGAGCGGAGG	This study	
3' UTR R primer: TTCACCACACTCCAGAAA	This study	
<i>SYNGAP1</i> ORF F primer: ATCGATGGATGAGAGCCGG	This study	
<i>SYNGAP1</i> ORF R primer: TTTGCTGGTTTCTCTCTCGG	This study	
Fragment analysis F primer: TGGAGCAGAGTGAGAAGAGGC	This study	
Fragment analysis R primer: GTCACACGCGGTTTGTG	This study	
<i>FUS</i> F primer: GTGGAGGCTATGAGGAGGT	This study	
<i>FUS</i> R primer: GCCTTACACTGGTTGCATT	This study	
<i>HNRNP</i> F primer: TGCTGTCTCATTCCACTGAC	This study	
<i>HNRNP</i> R primer: TTGGATCATAAGGCTGTGCA	This study	
<i>GAPDH</i> F primer: ACAGTCAGCCGATCTTCT	This study	
<i>GAPDH</i> R primer: ACGACCAATCCGTTGACTC	This study	
$\beta$ -Actin F primer: CTCTCCAGCCTTCTCTCT	This study	
$\beta$ -Actin R primer: TGTTGGCTACAGGCTCTTG	This study	
5' arm F primer for cloning <i>SYNGAP1</i> 3' UTR CAACTTTGTATAATAAAGTTGGAGAGGCAGCTCCCCCTTG	This study	
5' arm R primer for cloning <i>SYNGAP1</i> 3' UTR ATGATTATCTTTCTAGGGTTAAGAGTGGTAGAAGGAGAAGGA	This study	
3' arm F primer for cloning <i>SYNGAP1</i> 3' UTR CAGACTATCTTTCTAGGGTTAAATTTACTCCCTCCCCACCCA	This study	
3' arm R primer for cloning <i>SYNGAP1</i> 3' UTR CAACTTTGTATAGAAAAGTTGGAGCACTCCCTACCCTTGAGG	This study	
Oligonucleotides	Source	
<i>SYNGAP1</i> -ASO: CUGGGGGUCAAGAGAGGGC	This study	
Ctrl-ASO: AUGAGUGCCAGAGCAUGUC	This study	
E1-ASO: GGTCCCGGGGGUCAAGAG	This study	
E3-ASO: CAAGGGUCCUGGGGGUCA	This study	
shFUS #1: GGACAGCAGAAAGCTATA	This study	
shFUS #2: CGGACATGGCCTCAAACGA	This study	
shHNRNP #1: GCATTTAAAAGATCTAGAA	This study	
shHNRNP #2: GGTTCAGTCTGATGAAA	Liu et al. (2018)	
shCtrl: AATTCCTCGAACGTGTCACGT	This study	
Antibodies	Source	Identifier
Rabbit polyclonal anti-FUS antibody	Bethyl Laboratories	Catalog #A300-293A, RRID:AB_263409
Mouse monoclonal anti-FUS antibody	Santa Cruz Biotechnology	Catalog #sc-47711, RRID:AB_2105208
Rabbit polyclonal anti-PAN <i>SYNGAP1</i>	Thermo Fisher Scientific	Catalog #PA1-046, RRID:AB_2287112
Rabbit polyclonal anti- <i>SYNGAP1</i> $\alpha$ 1	Millipore	Catalog # 06-900, RRID:AB_11212750
Rabbit polyclonal anti- <i>SYNGAP1</i> $\alpha$ 2	Abcam	Catalog #ab77235, RRID:AB_1524465
Rabbit polyclonal anti-HNRNP	MBL international	Catalog #RN019P, RRID:AB_1953048
Mouse monoclonal anti-HNRNP	Santa Cruz Biotechnology	Catalog #sc-28380, RRID:AB_62773
Chicken polyclonal anti-CHAT	Aves Labs	Catalog #CAT, RRID:AB_2313537
Mouse monoclonal anti-HB9	DSHB	Catalog #MNR2, RRID:AB_2314625
Mouse monoclonal anti-ISL1	DSHB	Catalog #PCRP-ISL1-1D4, RRID:AB_2618777
Rabbit polyclonal anti- $\beta$ III-Tubulin	BioLegend	Catalog #845502, RRID:AB_2566589
Chicken polyclonal anti-MAP2	Abcam	Catalog #ab5392, RRID:AB_2138153
Mouse monoclonal anti-GAPDH	MBL International	Catalog #M171-3, RRID:AB_10597731
Rabbit polyclonal anti-ELAVL2	Proteintech	catalog # 14008-1-AP, RRID:AB_2096356
Mouse monoclonal anti-PUF60	GeneTex	Catalog #GTX629887, RRID:AB_2888176
Rabbit polyclonal anti-synaptophysin	Abcam	Catalog #ab32127, RRID:AB_2286949
Alexa Fluor 488 phalloidin	Thermo Fisher Scientific	N/A
Alexa Fluor 555 anti-chicken secondary antibody	Thermo Fisher Scientific	Catalog #A-21437, RRID:AB_2535858
Alexa Fluor 633 anti-rabbit secondary antibody	Thermo Fisher Scientific	Catalog #A-21070, RRID:AB_2535731
Alexa Fluor 633 anti-chicken secondary antibody	Thermo Fisher Scientific	Catalog #A-21103, RRID:AB_2535756
Alexa Fluor 488 anti-mouse IgG2a secondary antibody	Thermo Fisher Scientific	Catalog #A-21131, RRID:AB_2535771
Alexa Fluor 555 anti-mouse IgG1 sary antibody	Thermo Fisher Scientific	Catalog #A-21127, RRID:AB_2535769

*Quantitative analysis of immunofluorescence data*

The immunofluorescent signal intensity was measured by ZEN software (Zeiss). The quantification of spine number was performed as described previously (Yokoi et al., 2017). Regions of dendrites located 30–100  $\mu$ m from the cell soma that did not intersect with other dendrites were

selected. The numbers of spines, labeled with Alexa Fluor 488-conjugated phalloidin, were counted over a region of 20  $\mu$ m in length. The number of spines was counted independently, without sample information. Synaptophysin-positive F-actin particles were detected using Zen software. The differentiation efficacy of iPSC-derived motor neurons

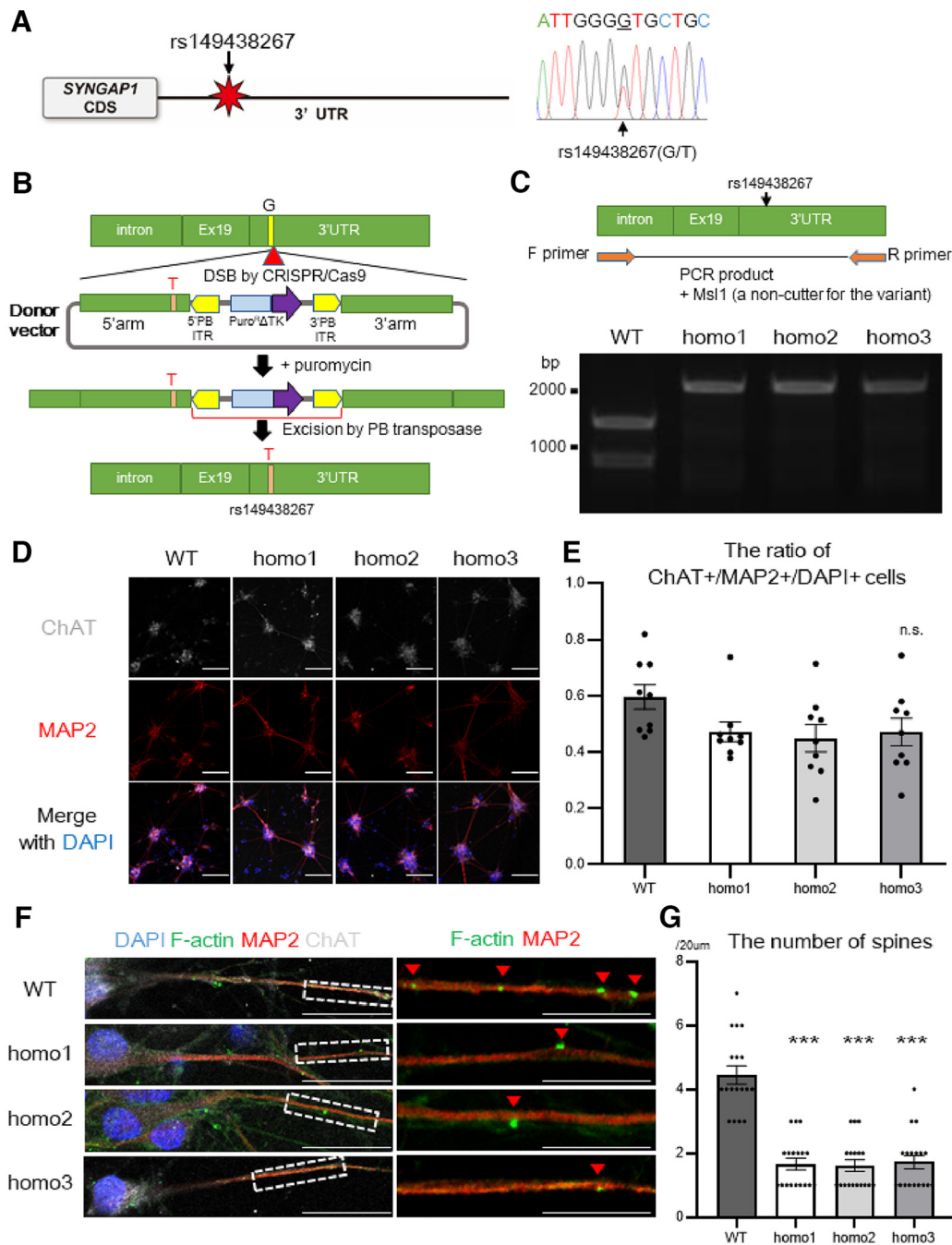


**Figure 1.** Motor neurons with the *SYNGAP1* rs149438267 homozygous mutation exhibit a loss of dendritic spines. **A**, The location of the *SYNGAP1* variant rs149438267 (g.33452118G>T, c.\*212G>T, GRCh38.p12; left). Sanger sequence of a patient with the *SYNGAP1* 3' UTR variant rs149438267 (right). Genomic DNA were extracted from peripheral blood leukocytes, and the heterozygous variant g.33452118G>T was confirmed. **B**, A schematic overview showing the strategy for scarless genome editing, inserting rs149438267 into iPSCs (201B7). **C**, RT-PCR was performed using primer sets to amplify DNA extracted from wild-type and edited homozygous iPSCs. PCR products were digested by *Msl*I, a noncutter for the *SYNGAP1* mutation, and analyzed by agarose gel electrophoresis. **D**, iPSC-derived motor neurons with the wild-type or homozygous mutation were cultured for four weeks and were immunostained for MAP2 (red), ChAT (white), and DAPI (blue). Scale bar: 10  $\mu$ m. **E**, Quantification of the ratio of ChAT/MAP2/DAPI-positive cells. Data are presented as the mean  $\pm$  SEM  $n$  = 9 fields, each from 3 independent wells; n.s., not significant, Kruskal–Wallis test, Bonferroni *post hoc* test. **F**, iPSC-derived motor neurons were immunostained for F-actin (green), MAP2 (red), and ChAT (white). Scale bars: 20  $\mu$ m for left columns, 10  $\mu$ m for right columns. **G**, Quantification of the number of spines per 20  $\mu$ m of dendrite length. Data are presented as the mean  $\pm$  SEM  $n$  = 18 each; \*\*\* $p$  < 0.001, one-way ANOVA, Tukey's *post hoc* test. Additional data of the FUS binding sites at *SYNGAP1* 3' UTR and induced pluripotent stem cell (iPSC)-derived motor neurons are displayed in Extended Data Figure 1-1.

was calculated by ImageJ. The intensities were calculated, and cells with intensities above the same threshold were considered positive.

### 3' RACE and TA-cloning

To identify the *SYNGAP1* 3' UTR variants, we used the SMARTer RACE 5'/3' kit (Takara) according to the manufacturer's instructions. The primer used in the assay was 5'-CTGTCCCAGGAAGAACAACAGCAA-3'.

The PCR products were inserted into the pRACE vector within the kit, and the sequences were analyzed.

### Immunocytochemistry and F-actin staining of neuronal cultures

Cultured motor neurons were immunostained as described previously (Yokoi et al., 2017), with some modifications. Samples were fixed with 4% paraformaldehyde at 37°C for 10 min, washed with PBS twice, and

blocked with 50% normal goat serum and 0.2% Triton X-100 (in PBS) for 30 min. Primary antibodies were diluted in 10% normal goat serum and 0.1% Triton X-100 (in PBS). After overnight incubation at 4°C with the primary antibodies, neurons were washed three times with PBS, and incubated with Alexa Fluor 488-, 555-, and 633-conjugated secondary antibodies (Invitrogen) at a dilution of 1:1000 for 2 h at room temperature. To evaluate spine morphology, F-actin was stained by Alexa Fluor 488-conjugated phalloidin (1:200, Invitrogen). Images were acquired with a microscope (LSM 710, Zeiss) at 40× or 100× magnification with oil immersion.

#### Western blotting

Samples were homogenized with brain immunoprecipitation buffer containing 25 mM HEPES-NaOH (pH 7.4), 150 mM NaCl, 5 mM MgCl<sub>2</sub>, 1 mM EDTA, and 1% NP-40. Protease inhibitors (Roche), phosphatase inhibitors (Thermo Fisher Scientific), and RNase inhibitors (Takara) were supplemented when needed. Homogenates were incubated on ice for 20 min and centrifuged at 13,000 rpm for 10 min at 4°C. The lysates were mixed with 4× NuPAGE lithium dodecyl sulfate (LDS) sample buffer (Novex), heated at 70°C for 5 min, and analyzed by Western blotting using the antibodies listed in Table 1. The band intensities were quantified using Multi Gauge 3.0 software (FujiFilm).

#### Immunoprecipitation

The total cell lysates were mixed with the antibodies and rotated at 4°C for 30 min. Protein-G Dynabeads (Invitrogen) were added to the mixture and further incubated at 4°C for 1.5 h. After washing the beads with Brain immunoprecipitation buffer three times, bound proteins or RNA were analyzed as below. The beads were directly mixed with NuPAGE LDS-PAGE sample buffer containing β-mercaptoethanol, heated at 95°C for 5 min, and analyzed with Western blotting. To analyze the bound RNA, the buffer was supplemented with RNase inhibitor (Takara). The beads after immunoprecipitation were incubated with 100-μl protein K buffer (100 mM Tris-HCl, pH 7.5, 12.5 mM EDTA, 150 mM NaCl, 1% SDS, 2 μg/μl protein K) for 15 min at 65°C. Then, Tris-EDTA buffer (200 μl) and phenol (300 μl) were added and vortexed vigorously. The RNA collected in the aqueous fraction was chloroform-washed and pelleted using ethanol precipitation with glycogen. The RNA was resuspended in distilled water and analyzed using quantitative RT-PCR.

#### Quantitative real-time PCR

RNA was prepared from motor neuron cultures using the Rneasy Mini kit (QIAGEN), according to the manufacturer's instructions. Total RNA was used as the template for reverse transcription using Superscript IV (Invitrogen). qRT-PCR was performed using the KAPA SYBR FAST qPCR kit (Kapa Biosystems), according to the manufacturer's instructions. RNA levels were normalized to those of β-actin mRNA.

#### DNA constructions

Targeting sequences of shRNA were listed in Table 1. These were cloned into a lentiviral shRNA vector (pLenti-RNAi-X2 puro DEST). For lentiviral *SYNGAP1* α1 and γ expression, the plasmid containing the human *SYNGAP1* α2 cDNA sequence (Dana form) was modified and cloned into the pLenti CMV-TO DEST puro vector with the FLAG tag. The sequences of shRNA were listed in Table 1. The sequence of shHNRNP2 was adapted from that previously reported (Liu et al., 2018).

#### Lentivirus production

Lentiviruses were produced as reported previously (Yokoi et al., 2017). The lentiviral transfer vector mentioned above with the packaging vectors pLP1, pLP2, and pVSVG was transfected into HEK293T cells. Lipofectamine 2000 in Opti-MEM was used for transfection according to the manufacturer's instructions. The medium was replaced with fresh Opti-MEM 1 d after transfection and collected with filtration 1 d later.

#### Statistical analyses

Western blotting, immunocytochemistry, immunoprecipitation, and qRT-PCR data were obtained from at least three independent experiments. All data were analyzed using IBM SPSS Statistics 27. Normality

**Table 2. The allele frequency of the *SYNGAP1* variant rs149438267**

Population	Allele count	Frequency of G/T allele <sup>a</sup>
JaCALS patient group	1614	0.00434*
JaCALS control group	382	0
ToMMo8.3KJPN	16,760	0.0017
GEM-JWGA <sup>b</sup>	14,452	0.0017
ToPMED (phase 3)	125,568	0.00014
gnomAD (v2.1.1)	31,136	0.000032
European (non-Finnish)	15,280	0.000065
African	8634	0
Latino	846	0
Ashkenazi Jewish	290	0
East Asian	1552	0
European (Finnish)	3458	0
Other	1076	0

\* $p < 0.05$  ( $p = 0.037$ , compared with ToMMo 8.3KJPN;  $p = 0.036$ , compared with GEM-J WGA, Fisher's exact test).

<sup>a</sup>All alleles are heterozygotes.

<sup>b</sup>The filter status of GEM-J WGA is not high confident region.

was determined using the Shapiro–Wilk test. For the statistical analysis of two groups, the unpaired *t* test was used. When the data were not distributed normally, the Mann–Whitney *U* test was used. In experiments with more than two groups, one-way analysis of variance (ANOVA) with the *post hoc* Tukey's multiple comparison test was used. When the data were not distributed normally, the Kruskal–Wallis test and *post hoc* Bonferroni test were used;  $\chi^2$  test and Fisher's exact test were used to test the independence of frequencies. In all experiments, the data are expressed as mean ± standard error of the mean (SEM), and the thresholds of statistical significance were set to  $p < 0.05$ ,  $p < 0.01$ , and  $p < 0.001$ .

## Results

### The *SYNGAP1* 3'UTR variant at the FUS binding site was identified in the Japanese ALS cohort

First, we referred to the CLIP-seq data of FUS in the human brain (Nakaya et al., 2013) for the FUS binding sites of human *SYNGAP1* 3'UTR. We found that most of the FUS CLIP tags were located in relative close proximity to exon 19, the 5' side of 3'UTR (Extended Data Fig. 1-1A), unlike the FUS CLIP tags in mice that are mostly located at the distant side to the exons at the 3' side of 3'UTR (Nakaya et al., 2013; Yokoi et al., 2017). This indicates that FUS regulation of *SYNGAP1* mRNA might differ between humans and mice. Based on these findings, we examined the *SYNGAP1* 3'UTR in the whole exome sequencing data of 807 Japanese patients with sporadic ALS and 191 normal controls registered in JaCALS database. We found eight variants in the *SYNGAP1* 3'UTR and the heterozygous *SYNGAP1* 3'UTR variant rs149438267 (G to T) in seven out of 807 ALS patients (1614 alleles), while it was absent in all 191 controls (382 alleles; Fig. 1A; Table 2), was the only variant at the FUS binding site. The allele frequency of this variant was 0.00434, which was significantly higher than those in the nation-wide Japanese database ToMMO8.3KJPN (0.0017,  $p = 0.037$ , Fisher's exact test) and GEMJ-WGA (0.0017,  $p = 0.036$ , Fisher's exact test; Tadaka et al., 2018; Table 2). Interestingly, the frequency of the variant was higher in the Japanese database compared with TOPMED or gnomAD (Karczewski et al., 2020), suggesting different incidence rates among different populations. In ALS patients with this variant, upper limb weakness or dysarthria were frequently observed as initial symptoms, whereas cognitive functions were well preserved (Table 3). The clinical courses were relatively rapid, especially in patients with dysarthria during the initial stage of the disease.

**Table 3. The clinical features of ALS patients with *SYNGAP1* variant rs149438267**

Sex	M	F	M	F	M	M	F
Age at onset	64	57	66	75	66	77	75
Clinical diagnosis based on the revised El Escorial criteria	Probable laboratory supported	Probable laboratory supported	Definite	Probable	Probable	Definite	Probable
Initial symptoms	Upper limb weakness	Upper limb weakness	Dysarthria	Upper limb weakness	Dysarthria, dysphagia, dyspnea	Dysarthria	Dysarthria
Duration from onset to death (month)	30	64	9	29 (censored observation)	7	18	38
Upper motor symptom	+	+	+	+	+	+	+
Lower motor symptom	+	+	+	+	+	+	+
Active denervation in EMG	+	+	+	+	+	+	+
Chronic denervation in EMG	+	+	+	+	+	+	–
Dementia	–	+	–	–	–	–	–
Cognitive tests	Not examined	MMSE 23, FAB 7	Not examined	MMSE 26, FAB 13	Not examined	MMSE 20, FAB 14	Not examined

### The *SYNGAP1* homozygous mutation induced a loss of dendritic spines

To reproduce the relationship between RNA-binding proteins and *SYNGAP1* 3'UTR by a single-nucleotide polymorphism (SNP) of noncoding sequence, we performed scarless genome editing by CRISPR-Cas9 and inserted the *SYNGAP1* 3'UTR variant rs149438267 into iPSCs in isogenic condition (Fig. 1B). We chose 201B7 because they have been well characterized (Takahashi et al., 2007) and because they are one of the most commonly and widely used high quality iPSCs (Imamura et al., 2017; Fujimori et al., 2018; Akiyama et al., 2019). First, we generated iPSCs carrying the rs149438267 variant in homozygosity to analyze the full genetic effect expressed by this polymorphism (Fig. 1C; Extended Data Fig. 1-1B). These screened iPSCs were then differentiated into motor neurons (Extended Data Fig. 1-1C; Shimojo et al., 2015; Onodera et al., 2020; Okada et al., 2021), and cell differentiation efficiencies were evaluated using the following procedure: after one week by immunocytochemistry of Islet-1 (ISL-1), homeobox protein HB9 (HB9), and  $\beta$ -III-tubulin (Extended Data Fig. 1-1D,E), and after four weeks by choline acetyltransferase (ChAT) and microtubule-associated protein 2 (MAP2; Fig. 1D,E). These data suggested that the differentiation efficiencies were similar in the wild-type (WT) and the homozygous mutant iPSC-derived motor neurons. Next, we evaluated spines in the motor neurons using F-actin immunolabeling (Extended Data Fig. 1-1F,G), and the number of F-actin particles was significantly decreased in the rs149438267 homozygous motor neurons (Fig. 1F,G). These results indicate that the *SYNGAP1* 3'UTR variant rs149438267 from patients with ALS is involved in the spine formation of motor neurons.

### The *SYNGAP1* homozygous mutant increased isoform $\alpha 1$ levels without altering total expression of *SYNGAP1*

*SYNGAP1* has four isoforms ( $\alpha 1$ ,  $\alpha 2$ ,  $\beta$ , and  $\gamma$ ), based on its spliced variant between exon 17, 18, and 19 (Fig. 2A; Jeyabalan and Clement, 2016; Kilinc et al., 2018). Each splice variant results in frameshifts and coded specific C-terminal amino acid sequences. Moreover, 3'UTR connected to each open reading frame (ORF) sequence is also known to have spliced variant in mice (Yokoi et al., 2017). First, we analyzed the spliced variants of *SYNGAP1* 3'UTR using rapid amplification of cDNA ends (RACE) of the RNA sequences from the WT iPSC-derived motor neurons. We found that short 3'UTR was present but to a lesser extent than full-length 3'UTR (Extended Data Fig. 2-1A). Cloning of RACE fragments revealed that the major ORF isoform of human *SYNGAP1* was  $\alpha 2$ , coinciding with that of mice

(Yokoi et al., 2017), and that the ORF isoform ratio between full-length 3'UTR and spliced short UTR was similar (Extended Data Fig. 2-1B). Unexpectedly, short UTR has many variations of potential spliced isoforms (Extended Data Fig. 2-1C). According to these data, we performed RT-PCR from *SYNGAP1*-ORF to the end of 3'UTR, and found no differences in the proportion of each isoform between the WT and the rs149438267 homozygous motor neurons (Fig. 2B). Although the *SYNGAP1* variant rs149438267 was located at the 3'UTR, the results suggest that this variant did not affect the splicing pattern of *SYNGAP1* 3'UTR.

Next, we focused on ORF expression of *SYNGAP1*. qRT-PCR of *SYNGAP1*-ORF revealed that ORF expression levels remained unchanged in the rs149438267 homozygous motor neurons (Fig. 2C). Western blotting showed an increase in *SYNGAP1* isoform  $\alpha 1$ , while PAN-*SYNGAP1* and *SYNGAP1*  $\alpha 2$  remained unchanged (Fig. 2D,E), suggesting that the increase in *SYNGAP1* isoform  $\alpha 1$  might be because of changes in alternative splicing. Note that the only commercially available antibodies are against PAN-*SYNGAP1* and  $\alpha 1$  and  $\alpha 2$  isoforms. We also generated iPSCs with the heterozygous mutation (Extended Data Fig. 2-1D) but could not detect the same alteration in *SYNGAP1* isoform expression (Extended Data Fig. 2-1E,F). This suggests that the heterozygous mutation might exert less effect on the *SYNGAP1* isoform under the current culture conditions.

*SYNGAP1* isoform  $\alpha 1$  is reported to decrease synaptic strength (Rumbaugh et al., 2006; McMahan et al., 2012), and we also reported that *SYNGAP1*  $\alpha 1$  overexpression decreases the number of mature spines in mouse primary hippocampal neurons (Yokoi et al., 2017). To confirm the effect of *SYNGAP1*  $\alpha 1$  on synaptic function, we overexpressed *SYNGAP1*  $\alpha 1$  in the WT motor neurons (Fig. 2F) and confirmed that *SYNGAP1*  $\alpha 1$  decreased the number of spines (Fig. 2G,H). These results suggest that an increase in *SYNGAP1*  $\alpha 1$  expression causes dendritic spine loss in the rs149438267 homozygous motor neurons.

### The *SYNGAP1* variant decreased *SYNGAP1* isoform $\gamma$ , which exerted a positive effect on spine formation

As mentioned above, *SYNGAP1* has four isoforms ( $\alpha 1$ ,  $\alpha 2$ ,  $\beta$ , and  $\gamma$ ) defined according to the alternative splicing between exons 17, 18, and 19. Because of the complexity of the isoform patterns, no study to date has evaluated all the isoforms simultaneously (Araki et al., 2020). To analyze how *SYNGAP1* variants change the alternative splicing of ORF, we performed fragment analysis of *SYNGAP1*-ORF between exon 17, 18, and 19 (Fig. 3A). Unexpectedly, we found a significant depletion of the isoform  $\gamma$  in the rs149438267 homozygous motor neurons, which could not be evaluated by Western blotting because of the lack of

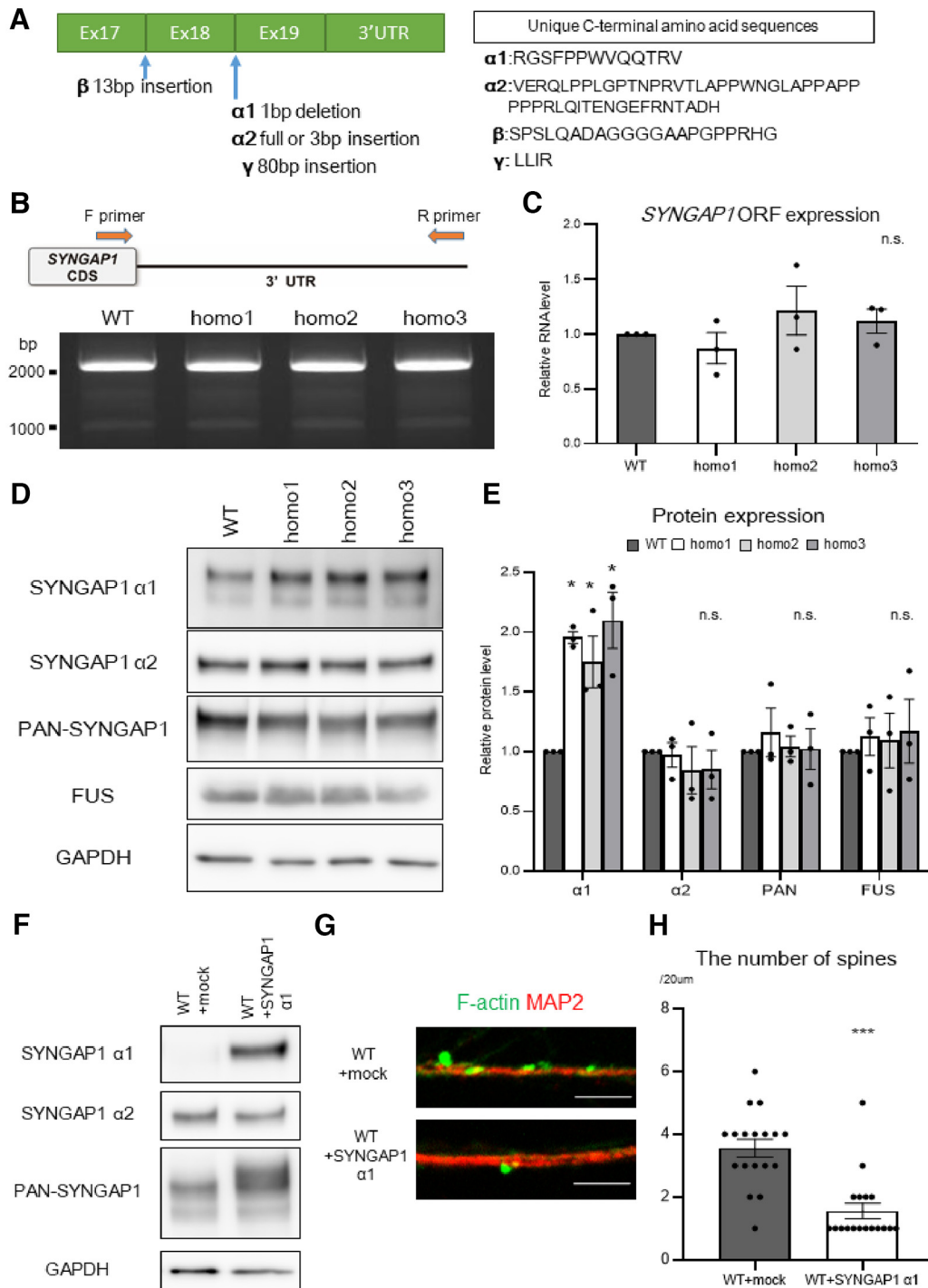


**Figure 2.** The *SYNGAP1* mutation increases isoform  $\alpha 1$  protein levels, which decreases the number of spines. **A**, A schematic overview of the spliced variant of *SYNGAP1* with C-terminal exons (green columns). **B**, RNA from wild-type and homozygous motor neurons was analyzed using RT-PCR to evaluate 3'UTR splicing. PCR products were analyzed with agarose electrophoresis to evaluate the 3'UTR variants. Representative data from triplicate experiments are shown. Additional data of *SYNGAP1* 3'UTR in iPSC-derived motor neurons are displayed in Extended Data Figure 2-1. **C**, RNA from wild-type and homozygous motor neurons was analyzed with qRT-PCR and the primer set for *SYNGAP1*-ORF. Data are presented as the mean  $\pm$  SEM  $n = 3$  each; n.s., not significant, one-way ANOVA, Tukey's *post hoc* test. **D**, The lysates from wild-type and homozygous iPSC-derived motor neurons were analyzed by Western blotting using the indicated antibodies. **E**, Quantification of the band intensities of the proteins in **D**.  $n = 3$ ; \* $p < 0.05$ ; n.s., not significant, one-way ANOVA, Tukey's *post hoc* test. **F**, Wild-type iPSC-derived motor neurons were infected with lentiviruses containing *SYNGAP1* isoform  $\alpha 1$  expression vector or mock vector. The lysates were analyzed by Western blotting using the indicated antibodies. Representative data from triplicate experiments are shown. **G**, Wild-type iPSC-derived motor neurons were infected with lentiviruses containing *SYNGAP1*  $\alpha 1$  expression vector or mock vector, and were immunostained for F-actin (green) and MAP2 (red). Scale bar: 5  $\mu$ m. **H**, Quantification of the number of spines per 20  $\mu$ m. Data are presented as the mean  $\pm$  SEM  $n = 18$  each; \*\*\* $p < 0.001$ , Mann–Whitney *U* test.

a specific antibody (Fig. 3B; Extended Data Fig. 3-1A,B). While a significant increase in isoform  $\alpha 1$  RNA levels in homozygous neurons was observed at the protein level (Fig. 2E), isoform  $\alpha 1$  RNA levels did not significantly increase in some lines (Fig. 3B;

Extended Data Fig. 3-1A,B). The isoform  $\gamma$  has also been found in mice brain (Araki et al., 2020); however, its function in spine formation has not been elucidated (Kilinc et al., 2018). Interestingly, the overexpression of the *SYNGAP1* isoform  $\gamma$



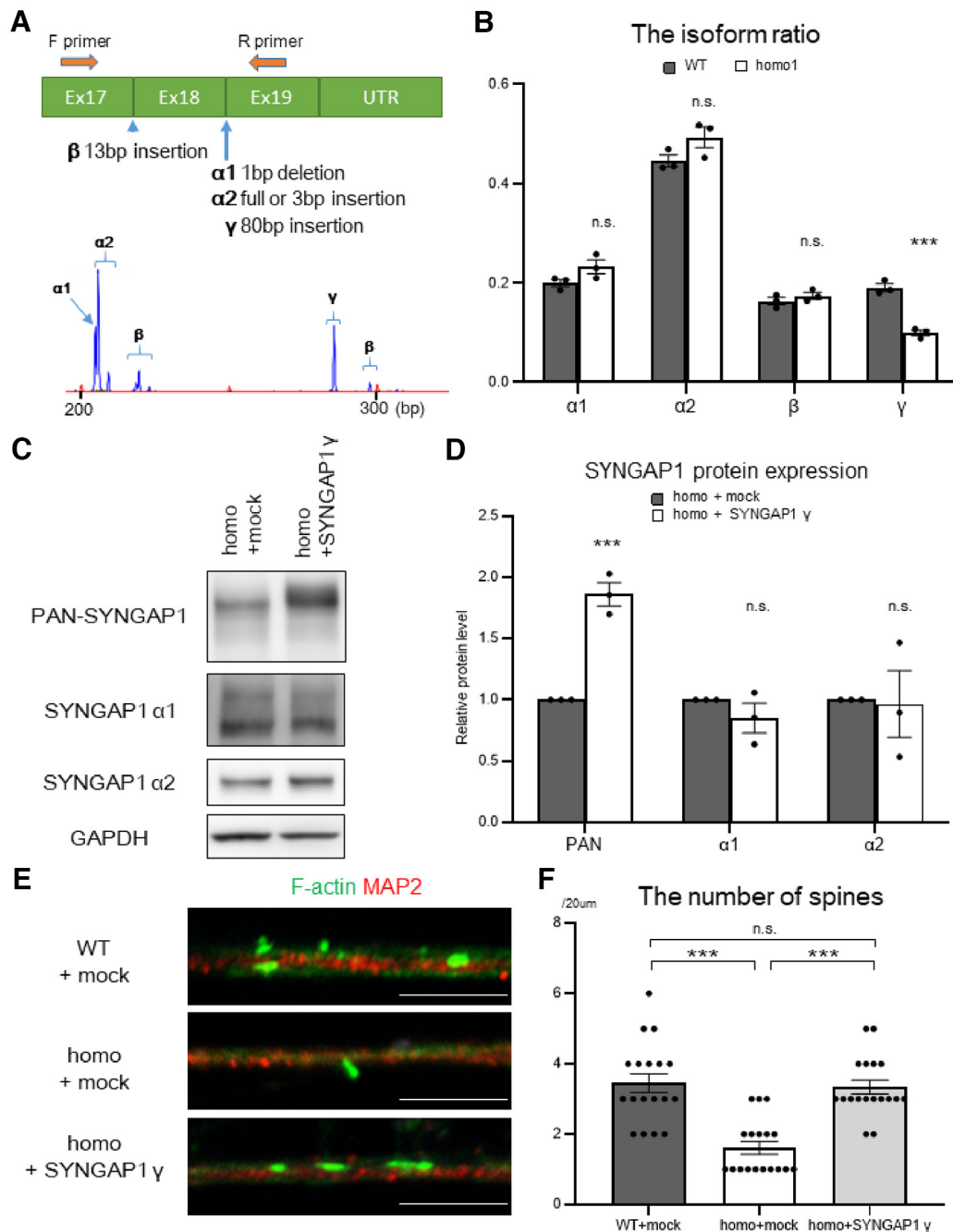


**Figure 3.** The *SYNGAP1* mutation decreases *SYNGAP1* isoform  $\gamma$  and thereby depletes the number of spines. **A**, A schematic overview of fragment analysis. The primer set was placed between exon 17 and exon 19 to evaluate spliced variants simultaneously. Representative raw data of fragment analysis are shown. **B**, RNA from wild-type or homozygous 1 (homo1; hereafter homo) motor neurons was analyzed with RT-PCR, and the PCR products were analyzed with fragment analysis. Data are presented as the mean  $\pm$  SEM  $n = 3$  each; \*\*\* $p$  < 0.001; n.s., not significant, unpaired  $t$  test. Additional data of the isoform changes in motor neurons with *SYNGAP1* homozygous mutation are displayed in Extended Data Figure 3-1. **C**, iPSC-derived motor neurons with the homozygous mutation were infected with lentiviruses expressing *SYNGAP1* isoform  $\gamma$  or mock. The lysates were analyzed with Western blotting using the indicated antibodies. **D**, Quantification of the band intensities of the proteins in **C**. Data are presented as the mean  $\pm$  SEM  $n = 3$ ; \*\*\* $p$  < 0.001; n.s., not significant, unpaired  $t$  test. **E**, Wild-type or homozygous iPSC-derived motor neurons were infected with lentiviruses expressing *SYNGAP1* isoform  $\gamma$  or mock, and were immunostained for F-actin (green) and MAP2 (red). Scale bar: 5  $\mu$ m. **F**, Quantification of the number of spines per 20  $\mu$ m. Data are presented as the mean  $\pm$  SEM  $n = 18$  each; \*\*\* $p$  < 0.001; n.s., not significant, Kruskal–Wallis test, Bonferroni *post hoc* test.

rescued a loss of dendritic spines in rs149438267 homozygous motor neurons (Fig. 3C–F), indicating that the *SYNGAP1* isoform  $\gamma$  is important for spine formation in motor neurons and can ameliorate spine abnormality in rs149438267 homozygous motor neurons, even in the presence of excess isoform  $\alpha 1$ . These results suggest that the aberrant splicing, an increase in isoform  $\alpha 1$  and a decrease in isoform  $\gamma$ , cause spine loss in the rs149438267 homozygous motor neurons.

### The *SYNGAP1* 3'UTR mutation excessively recruited FUS and HNRNPK

To clarify how the *SYNGAP1* 3'UTR variant rs149438267 affects the aberrant splicing of *SYNGAP1* isoforms  $\alpha 1$  and  $\gamma$ , we next evaluated the binding efficacy of FUS and collaborating RNA-binding proteins. We generated biotinylated RNA probes with 240-nt sequences for the 5' side of *SYNGAP1* 3'UTR with or without the mutation (Fig. 4A), and performed RNA pull-down

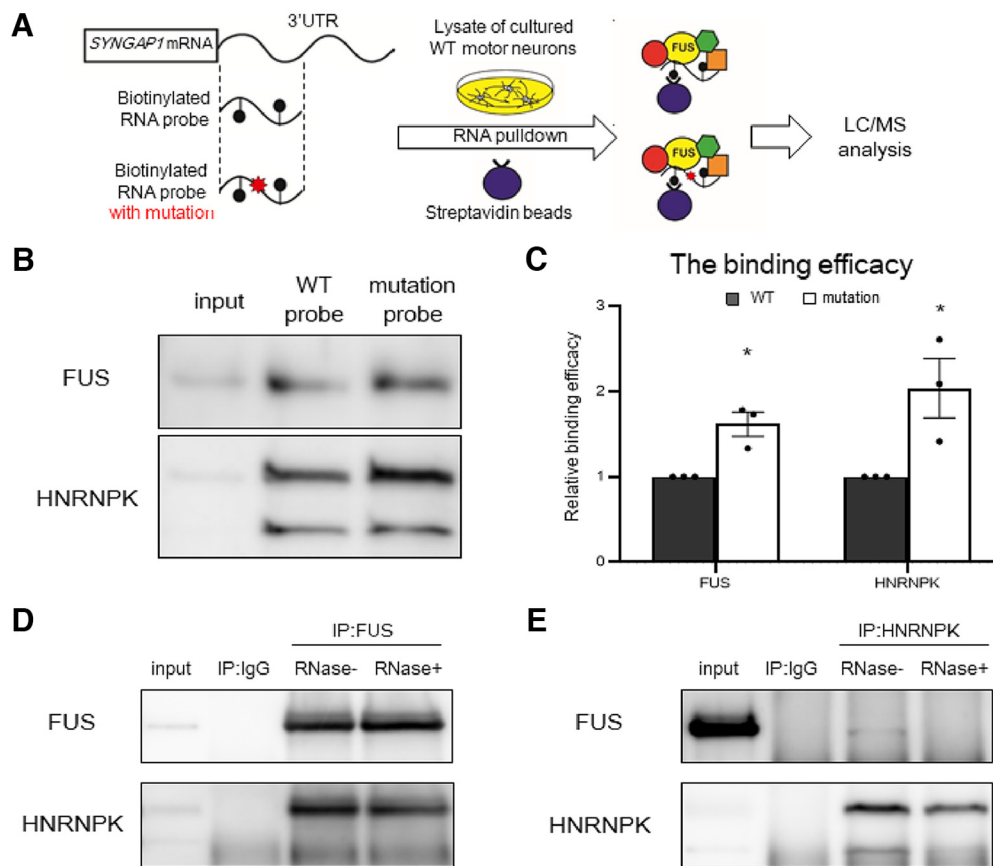


**Figure 4.** The *SYNGAP1* 3'UTR mutation excessively recruits FUS and HNRNPK. **A**, A scheme of the biotinylated RNA pull-down assay using *SYNGAP1* mRNA 3'UTR sequences followed by mass spectrometry analysis. **B**, RNA pull-down assay was performed with a biotinylated RNA probe cloned from the *SYNGAP1* 3'UTR. Pull-down samples were analyzed by Western blotting using the indicated antibodies. **C**, Quantification of the band intensities in **B**. Data are presented as the mean  $\pm$  SEM  $n = 3$ ;  $*p < 0.05$ , unpaired  $t$  test. Additional data of pull-down assay and HNRNPK protein expression are displayed in Extended Data Figure 4-1 and Extended Data Table 4-1. **D**, **E**, Co-immunoprecipitation (Co-IP) of FUS (**D**) and HNRNPK (**E**) using lysates from wild-type motor neurons with or without RNase A treatment. The bound proteins were detected with Western blotting and the indicated antibodies. Representative data from triplicate experiments are shown.

assay to analyze the binding efficacy of RNA-binding proteins to each probe by Western blotting. Interestingly, the binding efficacy of FUS to the probe with the mutation was increased compared with the probe without the mutation (Fig. 4B,C), suggesting that the *SYNGAP1* 3'UTR variant rs149438267 recruited FUS to 3'UTR. In addition to FUS, gel digestion and LC/MS analysis of the specific bands in each sample were performed to examine the proteins that bind to the *SYNGAP1* 3'UTR (Extended Data Fig. 4-1A; Extended Data Table 4-1). We found that the binding efficacy of heterogeneous nuclear ribonucleoprotein K (HNRNPK) also increased with the mutated probe (Fig. 4B,C). HNRNPK is a DNA/RNA-binding protein that plays important roles in transcription (Michelotti et al., 1996; Wang et al., 2020), paraspeckle formation (Fox et al., 2018), splicing (Liu et al., 2018; Thompson et al., 2018), and post-transcriptional regulation at 3'UTR (Yano et al., 2005; Liepelt et al., 2014; Shin et al., 2017). The relationships between HNRNPK and diseases such as cancer (Barboro et al., 2014), Kabuki-like syndrome (Dentici et al., 2018), and Au-Kline syndrome (Au et al., 2018) have been described. The anti-HNRNPK antibody recognizes two splice variants (Barboro et al., 2009). We also analyzed other candidates found in the LC/MS analysis, including ELAVL2 and PUF60, which remained unchanged (Extended Data Fig. 4-1B, C). Importantly, HNRNPK is also known to interact with FUS (Groen et al., 2013). The expression level of HNRNPK remained unchanged between the WT and the rs149438267 homozygous

motor neurons (Extended Data Fig. 4-1D,E). To validate whether FUS and HNRNPK bind to *SYNGAP1* mRNA, we performed RNA-IP of the motor neuron cultures using the antibodies for each RNA-binding protein. The binding efficacy of *SYNGAP1* mRNA to FUS and HNRNPK tended to be higher in the rs149438267 homozygous motor neurons than in the WT motor neurons (Extended Data Fig. 4-1F-I). Moreover, co-immunoprecipitation assay (Co-IP) by the anti-FUS antibody with the RNase A treatment revealed that FUS and HNRNPK bound with each other via protein-protein interactions (Fig. 4D). Co-IP by anti-HNRNPK antibody showed that the level of FUS bound to HNRNPK was low and reduced by RNase A treatment. This suggests that HNRNPK is not always bound to FUS, and that some of the FUS proteins bind to HNRNPK via protein-protein interactions and others bind indirectly to HNRNPK via RNA. These results suggest that HNRNPK is a crucial collaborator of FUS, and that both proteins are excessively recruited by the *SYNGAP1* 3'UTR variant.

#### HNRNPK, rather than FUS, altered the expression pattern of *SYNGAP1* isoforms

Next, we performed knock-down experiments to elucidate how FUS and HNRNPK regulate *SYNGAP1* isoforms. It should be noted that after HNRNPK knock-down, motor neurons could not survive for four weeks, and thus we collected samples on day 14. Western blot analysis (Fig. 5A-D) showed that FUS knock-

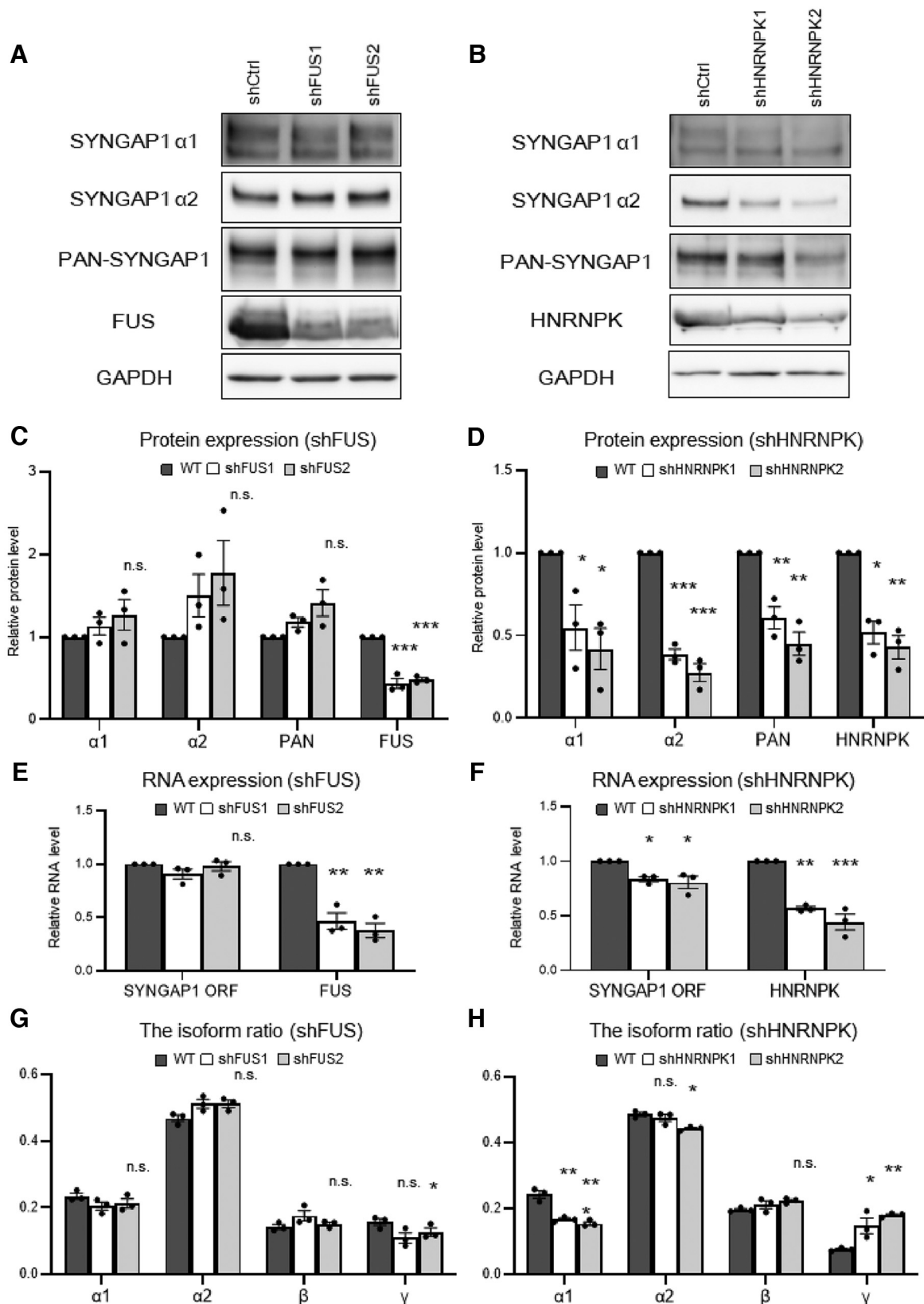


**Figure 5.** HNRNPK, rather than FUS, alters SYNGAP1 isoforms similar to those observed in motor neurons with the rs149438267 homozygous mutation. **A, B**, The lysates from wild-type motor neurons infected with shCtrl, shFUS1, and shFUS2 (**A**) or shCtrl, shHNRNPK1, and shHNRNPK2 (**B**;  $n = 3$ ) were subjected to Western blotting with the indicated antibodies. **C, D**, Quantification of the band intensities of the indicated proteins in **A, B**. Data are presented as the mean  $\pm$  SEM ( $n = 3$ ; \* $p < 0.05$ , \*\* $p < 0.01$ , \*\*\* $p < 0.001$ , one-way ANOVA, Tukey's *post hoc* test. **E, F**, Total RNA was extracted from wild-type motor neurons infected with shCtrl, shFUS1, and shFUS2 (**E**) or shCtrl, shHNRNPK1, and shHNRNPK2 (**F**;  $n = 3$  neuron cultures each), and the mRNA expression levels of SYNGAP1, FUS, and HNRNPK were analyzed with qRT-PCR. Data are presented as the mean  $\pm$  SEM; \* $p < 0.05$ , \*\* $p < 0.01$ , \*\*\* $p < 0.001$ , one-way ANOVA, Tukey's *post hoc* test. **G, H**, Total RNA from wild-type motor neurons infected with shCtrl, shFUS1, and shFUS2 (**G**;  $n = 4$ ) or shCtrl, shHNRNPK1, and shHNRNPK2 (**H**;  $n = 3$ ) was analyzed with

down did not result in significant changes in *SYNGAP1* expression levels (Fig. 5C). More importantly, HNRNPK knock-down decreased PAN-*SYNGAP1* as well as isoforms  $\alpha 1$  and  $\alpha 2$  (Fig. 5D). qRT-PCR revealed that HNRNPK knock-down, but not FUS knock-down, decreased the total expression of *SYNGAP1*-ORF (Fig. 5E,F), consistent with the results of Western blotting (Fig. 5C,D). Fragment analysis also revealed that HNRNPK knock-down decreased isoform  $\alpha 1$  and increased isoform  $\gamma$  levels, while FUS knock-down slightly decreased isoform  $\gamma$  levels (Fig. 5G,H). HNRNPK knock-down also induced another undescribed alternative splicing variant, which could be translated into isoform  $\gamma$  but had longer intron sequences than the conventional  $\gamma$  sequence (Extended Data Fig. 5-1A). These results indicate HNRNPK-controlled alternative splicing of *SYNGAP1* mRNA, especially isoform  $\gamma$ . In addition, the changes in *SYNGAP1* expression or isoform alteration in the double-knock-down of FUS and HNRNPK were similar to those in the HNRNPK knock-down model (Extended Data Fig. 5-1B-E), which suggests that HNRNPK plays a major role in controlling *SYNGAP1* expression. FUS had no significant effect on the transcript levels of *SYNGAP1* variants, but it affected *SYNGAP1*  $\alpha 1$  protein expression, which was decreased in the HNRNPK knock-down but not in the double-knock-down. Given that the *SYNGAP1* variant rs149438267 caused aberrant splicing, thus increasing isoform  $\alpha 1$  and decreasing isoform  $\gamma$ , these results indicate that HNRNPK, rather than FUS, might contribute to the altered splicing of *SYNGAP1* isoforms through the variant. However, the knock-down experiments could not directly explain the relationship between the excessive recruitment of RNA-binding proteins, aberrant splicing, and dendritic spine loss.

### The antisense oligonucleotides toward the HNRNPK binding sites ameliorated spine abnormalities

To further elucidate how the excessive recruitment of HNRNPK contributes to the aberrant splicing and dendritic spine loss in the rs149438267 homozygous motor neurons, we considered blocking the recruitment of RNA-binding proteins with antisense oligonucleotides (ASOs), which may represent a therapeutic reagent for ALS (Kole et al., 2012; Bennett et al., 2019). According to the eCLIP of K562 cells from the ENCODE datasets (Davis et al., 2018), the *SYNGAP1* 3'UTR variant rs149438267 was located between the putative FUS and HNRNPK binding sites (Extended Data Fig. 6-1A). Moreover, the RegRNA database showed that the exonic splicing enhancer was present at the 3' side of the variant (Chang et al., 2013), and the mCrossBase database showed that the HNRNPK binding motifs were distributed around the exonic splicing enhancer (Feng et al., 2019; Fig. 6A).

Referring to these data, we designed three ASOs toward *SYNGAP1* 3'UTR (E1, E2, and E3) and treated the rs149438267 homozygous motor neurons with 10 or 50 nM of these ASOs, followed by evaluation after 14 d (Extended Data Fig. 6-1B). We then selected E2-ASO as *SYNGAP1*-ASO, which exhibited an increase of *SYNGAP1* isoform  $\gamma$  at 50 nM, as observed using fragment analysis in a single experiment (Extended Data Fig. 6-1C,D). Pull-down assay confirmed that *SYNGAP1*-ASO could

block the excessive binding of HNRNPK to the probe with the *SYNGAP1* 3'UTR mutation (Fig. 6B,C). Unexpectedly, *SYNGAP1*-ASO significantly increased the binding efficacy of FUS to the mutation probe (Extended Data Fig. 6-1E,F). Moreover, pull-down assay of HNRNPK knock-down showed that the depletion of HNRNPK did not increase FUS binding to the mutation probe (Extended Data Fig. 6-1G,H), which suggests that HNRNPK and FUS interact indirectly at *SYNGAP1* 3'UTR, and that ASO independently blocked HNRNPK and increased FUS binding. Next, we analyzed the effects of *SYNGAP1*-ASO on the expression pattern of the *SYNGAP1* isoforms. Fragment analysis revealed that the treatment of *SYNGAP1*-ASO for 14 d in the rs149438267 homozygous motor neurons increased the expression ratio of isoform  $\gamma$ , decreased the expression ratio of isoform  $\alpha 2$ , and did not alter the expression ratio of isoform  $\alpha 1$  (Fig. 6D). qRT-PCR revealed that the expression level of total *SYNGAP1* was not affected by *SYNGAP1*-ASO (Fig. 6E), suggesting that *SYNGAP1*-ASO could solely affect the alternative splicing of *SYNGAP1* isoforms. In addition, *SYNGAP1*-ASO did not alter the *SYNGAP1* isoforms in WT neurons 14 d after ASO treatment (Extended Data Fig. 6-1G,H), suggesting that *SYNGAP1*-ASO could specifically correct the excessive recruitment of HNRNPK induced by the variant. Western blotting showed that the expression of *SYNGAP1*  $\alpha 2$  was decreased in the rs149438267 homozygous motor neurons 14 d after *SYNGAP1*-ASO treatment, while *SYNGAP1*  $\alpha 1$  and PAN-*SYNGAP1* remained unchanged (Fig. 6F,G), consistent with the results of fragment analysis (Fig. 6D).

Finally, *SYNGAP1*-ASO treatment for 14 d could ameliorate a loss of dendritic spines in the rs149438267 homozygous motor neurons (Fig. 6H,I). This suggests that the excessive recruitment of HNRNPK was the major pathogenic mechanism for dendritic spine loss in the rs149438267 homozygous motor neurons. Together, these results clarify that the *SYNGAP1* 3'UTR variant rs149438267 identified in the Japanese ALS cohort excessively recruits RNA-binding proteins, especially HNRNPK, and causes a loss of dendritic spines in iPSC-derived motor neurons (Fig. 7).

## Discussion

In this study, we screened ALS patients in a combined Japanese cohort at the FUS binding site in the *SYNGAP1* 3'UTR. We found the variant rs149438267 was associated with a loss of dendritic spines in iPSC-derived motor neurons. While previous studies have demonstrated that *SYNGAP1* is a pathogenic candidate for autism spectrum disorder (Mignot et al., 2016), no report to date has demonstrated a relationship between *SYNGAP1* and ALS. Interestingly, *SYNGAP1* mutations in individuals with autism spectrum disorder represent loss-of-function mutations (Mignot et al., 2016), and *Syngap1* hetero knock-out mice show an increase in the proportion of mature spines (Clement et al., 2012). Our findings of spine loss by *SYNGAP1* 3'UTR variant rs149438267 differ from the function of *SYNGAP1* observed in previous research. Synapse loss has been reported as an early pathologic feature of neurodegenerative diseases, including ALS (Sasaki and Maruyama, 1994; Herms and Dorostkar, 2016; Henstridge et al., 2018). Also, synaptic dysfunction has been reported to contribute to early motor and cognitive dysfunctions before neuronal death in a mouse model of ALS/FTLD (Sunico et al., 2011; Yokoi et al., 2017). In this study, we confirm the presence of dendritic spine loss by the *SYNGAP1* 3'UTR rs149438267 in iPSC-derived homozygous motor neurons, which could help to elucidate the pathogenesis of early-stage ALS.

←

RT-PCR and fragment analysis to evaluate the change in the *SYNGAP1* isoform ratio. Data are presented as the mean  $\pm$  SEM; \* $p < 0.05$ , \*\* $p < 0.01$ , \*\*\* $p < 0.001$ , one-way ANOVA, Tukey's *post hoc* test. Additional data of altered *SYNGAP1* splicing by HNRNPK are displayed in Extended Data Figure 5-1.

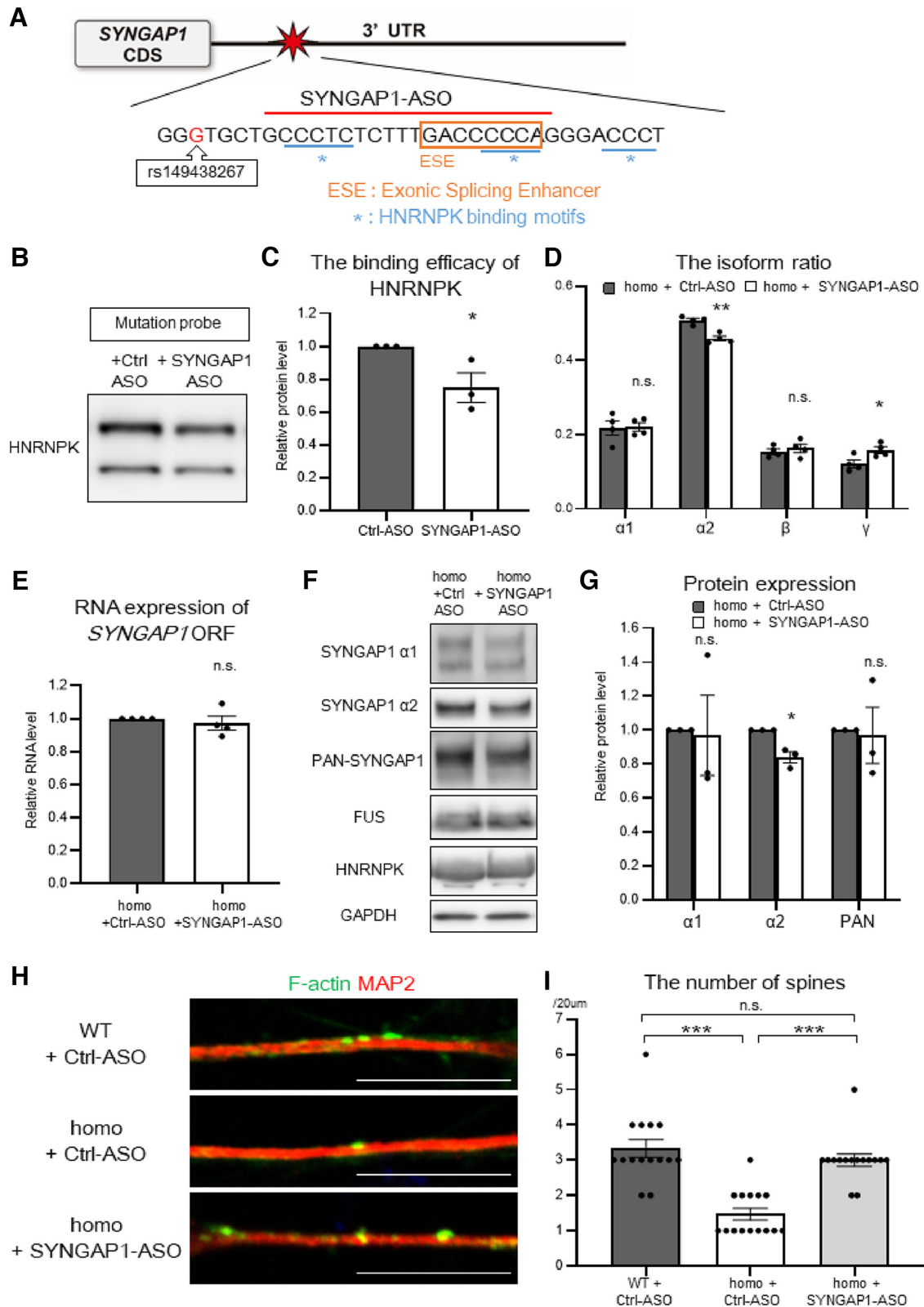


**Figure 6.** Antisense oligonucleotides blocked the HNRNPK binding site and ameliorated a loss of dendritic spines. **A**, A schematic overview of antisense oligonucleotides toward SYNGAP1 3' UTR. The scheme shows the sequences representing the binding motifs of HNRNPK according to the mCrossBase database (underlined in blue) and the exonic splicing enhancer according to the RegRNA database (orange frame). **B**, RNA pull-down assay was performed with the lysates from the wild-type motor neurons and biotinylated RNA probe with rs149438267. Pull-down samples were analyzed by Western blotting using the indicated antibodies. **C**, Quantification of the band intensities in **B**. Data are presented as the mean  $\pm$  SEM  $n = 3$  each;  $*p < 0.05$ , unpaired  $t$  test. **D**, Fragment analysis of RNA extracted from motor neurons with the homozygous mutation 14 d after Ctrl-ASO or SYNGAP1-ASO treatment. Data are presented as the mean  $\pm$  SEM  $n = 4$  each;  $**p < 0.01$ ,  $*p < 0.05$ ; n.s., not significant, unpaired  $t$  test. **E**, RNA samples (same as in **D**) were analyzed with RT-PCR and the primer set for SYNGAP1-ORF. Data are presented as the mean  $\pm$  SEM  $n = 4$  each; unpaired  $t$  test. **F**, Motor neurons with the homozygous mutation were treated with Ctrl-ASO or SYNGAP1-ASO for 14 d and were then subjected to Western blotting with the indicated antibodies. **G**, Quantification of the band intensities of the proteins in **F**. Data are presented as the mean  $\pm$  SEM  $n = 3$ ;  $*p < 0.05$ ; n.s., not significant,

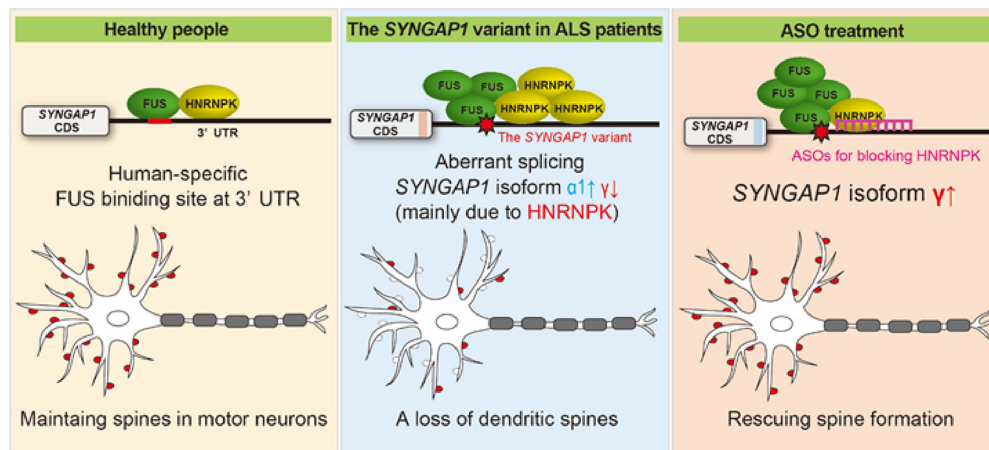


**Figure 7.** The *SYNGAP1* 3'UTR variant excessively recruits HNRNPK, causing aberrant *SYNGAP1* splicing and dendritic spine loss. A graphical summary of the mechanism of dendritic spine loss by the *SYNGAP1* 3'UTR variant. The *SYNGAP1* 3'UTR variant excessively recruits RNA-binding proteins, causing aberrant *SYNGAP1* splicing and dendritic spine loss. ASOs that block HNRNPK recruitment increase expression of the *SYNGAP1* isoform  $\gamma$  and ameliorate the loss of dendritic spines, which suggests that HNRNPK plays an important role in dendritic spine loss of motor neurons with the *SYNGAP1* 3'UTR variant.

We found that the *SYNGAP1* 3'UTR rs149438267 variant excessively recruited FUS and HNRNPK. Interestingly, the cooperative protein with FUS is quite different from that in mice (Yokoi et al., 2017). Moreover, we found that ASO, which blocks the excessive recruitment of HNRNPK to *SYNGAP1* 3'UTR, could alter the *SYNGAP1* splicing, and ameliorate dendritic spine loss in the rs149432867 homozygous motor neurons. This result emphasizes that excess HNRNPK recruitment is the crucial mechanism underlying dendritic spine formation in motor neurons. *SYNGAP1* 3'UTR contains exonic splicing enhancers close to the HNRNPK binding site, and HNRNPK is known to affect the association between RNA-binding proteins and exonic splicing enhancers or silencers (Marchand et al., 2011). The variants at the 3'UTR have been reported to affect the alternative splicing of ORF (Zhao et al., 2019). Because of such splicing machinery, the excessive binding of HNRNPK itself or HNRNPK and other collaborating RNA-binding proteins could have introduced the aberrant splicing in the rs149432867 homozygous motor neurons.

We also found that HNRNPK affected the *SYNGAP1* isoform  $\gamma$ . *SYNGAP1* has four isoforms, of which isoform  $\alpha 1$  is the most validated isoform that has a PDZ domain that interacts with proteins at the postsynaptic density and regulates synaptic plasticity (Kim et al., 1998; Araki et al., 2015). There have been few reports on the function of *SYNGAP1* isoform  $\gamma$  (Araki et al., 2020). Our findings indicate that the *SYNGAP1* isoform  $\gamma$  plays an important role in spine formation in human models. While the *SYNGAP1* isoform  $\gamma$  was increased,  $\alpha 1$  remained unchanged, and  $\alpha 2$  was decreased by ASO treatment. Together with the results of double-knock-down of FUS and HNRNPK, this indicates that FUS affects HNRNPK-dependent alteration of the *SYNGAP1*  $\alpha 1$  level. Although the decrease in the *SYNGAP1* isoform  $\alpha 2$  might have suppressed synaptic strength (McMahon et al., 2012), the decrease in  $\alpha 1$  and increase in  $\gamma$  improved spine

abnormality, possibly by overcoming the effects of  $\alpha 2$ . Also, ASO could ameliorate spine loss without sequestering FUS from *SYNGAP1* 3'UTR by ASO. These data indicate that HNRNPK regulation of the *SYNGAP1* isoform  $\gamma$ , which is independent of FUS and *SYNGAP1* isoform  $\alpha 1$ , is a crucial mechanism underlying spine abnormality caused by the *SYNGAP1* 3'UTR rs149438267 variant. Further evaluations in motor neurons with FUS mutation are needed to elucidate whether FUS has the pathogenic correlation with *SYNGAP1*.

In this study, there were some discrepancies between the Western blot and fragment analysis results in the evaluation of *SYNGAP1*  $\alpha$  isoforms. These could be a result of translational control of *SYNGAP1* mRNA (Popovitchenko et al., 2020) or isoform-specific protein stability control (Vuong et al., 2022). Since there was a difference of only one base pair between isoform  $\alpha 1$  and  $\alpha 2$ , it is difficult to distinguish each mRNA to analyze translational control. Moreover, given that *SYNGAP1* isoforms are defined within a long region of alternative splicing between exons 17, 18, and 19, it is difficult to evaluate all isoforms simultaneously, even with next-generation sequencing (Araki et al., 2020). These discrepancies might be also because of the insufficient detection capability of fragment analysis. In addition, protein expression of isoforms  $\beta$  and  $\gamma$  could not be analyzed because of the absence of specific antibodies. Further developments in methods to elucidate the regulation of *SYNGAP1* isoforms are expected.

We could not confirm aberrant *SYNGAP1* alterations in the rs149432867 heterozygous motor neurons. This might be because of the experimental settings, e.g., the duration of motor neuron culturing or the composition of the motor neuron medium (Bardy et al., 2015; Odawara et al., 2016). In addition, we could not generate iPSCs from patients with the *SYNGAP1* variants rs149432867 because of ethical limitations. We could not obtain informed consent from patients with *SYNGAP1* variant rs149432867 to generate iPSCs from their samples. It should also be noted that the heterozygous variant might have milder pathologies than the homozygous variant. Thus, a more detailed analysis of heterozygous motor neurons is needed to fully demonstrate the relevance of this variant in the pathogenesis of ALS.

In summary, we identified the *SYNGAP1* 3'UTR variant rs149432867 from the Japanese sporadic ALS cohort as a major

←  
unpaired *t* test. **H**, Motor neurons were immunostained for F-actin (green) and MAP2 (red). Scale bars: 10  $\mu$ m. **I**, Quantification of the number of spines per 20  $\mu$ m. Data are presented as the mean  $\pm$  SEM *n* = 15 each; \*\*\**p* < 0.001, n.s. not significant, Kruskal–Wallis test, Bonferroni *post hoc* test. The fundamental data of *SYNGAP1*-ASO toward the binding site of HNRNPK are displayed in Extended Data Figure 6-1.

candidate involved in a loss of dendritic spines in iPSC-derived motor neurons. In addition, we demonstrated that the *SYNGAP1* 3'UTR variant altered *SYNGAP1* isoforms via the excess recruitment of FUS and HNRNP; in particular, HNRNP played an important role in *SYNGAP1* splicing and spine formation. Our findings provide a basis for the future exploration of ALS-related RNA-binding proteins.

## References

- Akiyama T, et al. (2019) Aberrant axon branching via Fos-B dysregulation in FUS-ALS motor neurons. *EBioMedicine* 45:362–378.
- Araki Y, Zeng M, Zhang M, Haganir RL (2015) Rapid dispersion of SynGAP from synaptic spines triggers AMPA receptor insertion and spine enlargement during LTP. *Neuron* 85:173–189.
- Araki Y, Hong I, Gamache TR, Ju S, Collado-Torres L, Shin JH, Haganir RL (2020) SynGAP isoforms differentially regulate synaptic plasticity and dendritic development. *Elife* 9:e56273.
- Au PYB, Goedhart C, Ferguson M, Breckpot J, Devriendt K, Wierenga K, Fanning E, Grange DK, Graham GE, Galarreta C, Jones MC, Kini U, Stewart H, Parboosingh JS, Kline AD, Innes AM; Care for Rare Canada Consortium (2018) Phenotypic spectrum of Au-Kline syndrome: a report of six new cases and review of the literature. *Eur J Hum Genet* 26:1272–1281.
- Barboro P, Repaci E, Rubagotti A, Salvi S, Boccardo S, Spina B, Truini M, Introini C, Puppo P, Ferrari N, Carmignani G, Boccardo F, Balbi C (2009) Heterogeneous nuclear ribonucleoprotein K: altered pattern of expression associated with diagnosis and prognosis of prostate cancer. *Br J Cancer* 100:1608–1616.
- Barboro P, Ferrari N, Balbi C (2014) Emerging roles of heterogeneous nuclear ribonucleoprotein K (hnRNP K) in cancer progression. *Cancer Lett* 352:152–159.
- Bardy C, van den Hurk M, Eames T, Marchand C, Hernandez RV, Kellogg M, Gorris M, Galet B, Palomares V, Brown J, Bang AG, Mertens J, Böhnke L, Boyer L, Simon S, Gage FH (2015) Neuronal medium that supports basic synaptic functions and activity of human neurons in vitro. *Proc Natl Acad Sci USA* 112:E27252E2734.
- Bennett CF, Krainer AR, Cleveland DW (2019) Antisense oligonucleotide therapies for neurodegenerative diseases. *Annu Rev Neurosci* 42:385–406.
- Chang TH, Huang HY, Hsu JB, Weng SL, Horng JT, Huang HD (2013) An enhanced computational platform for investigating the roles of regulatory RNA and for identifying functional RNA motifs. *BMC Bioinformatics* 14 [Suppl 2]:S4.
- Clement JP, Aceti M, Creson TK, Ozkan ED, Shi Y, Reish NJ, Almonte AG, Miller BH, Wiltgen BJ, Miller CA, Xu X, Rumbaugh G (2012) Pathogenic *SYNGAP1* mutations impair cognitive development by disrupting maturation of dendritic spine synapses. *Cell* 151:709–723.
- Davis CA, Hitz BC, Sloan CA, Chan ET, Davidson JM, Gabdank I, Hilton JA, Jain K, Baymuradov UK, Narayanan AK, Onate KC, Graham K, Miyasato SR, Dreszer TR, Strattan JS, Jolanki O, Tanaka FY, Cherry JM (2018) The encyclopedia of DNA elements (ENCODE): data portal update. *Nucleic Acids Res* 46:D794–D801.
- Dentici ML, Barresi S, Niceta M, Pantaleoni F, Pizzi S, Dallapiccola B, Tartaglia M, Digilio MC (2018) Clinical spectrum of Kabuki-like syndrome caused by HNRNP haploinsufficiency. *Clin Genet* 93:401–407.
- Deshpande D, Higelin J, Schoen M, Vomhof T, Boeckers TM, Demestre M, Michaelis J (2019) Synaptic FUS localization during motoneuron development and its accumulation in human ALS synapses. *Front Cell Neurosci* 13:256.
- Feng H, Bao S, Rahman MA, Weyn-Vanhenhenryck SM, Khan A, Wong J, Shah A, Flynn ED, Krainer AR, Zhang C (2019) Modeling RNA-binding protein specificity in vivo by precisely registering protein-RNA crosslink sites. *Mol Cell* 74:1189–1204.e6.
- Fox AH, Nakagawa S, Hirose T, Bond CS (2018) Paraspeckles: where long noncoding RNA meets phase separation. *Trends Biochem Sci* 43:124–135.
- Fujii R, Okabe S, Urushido T, Inoue K, Yoshimura A, Tachibana T, Nishikawa T, Hicks GG, Takumi T (2005) The RNA binding protein TLS is translocated to dendritic spines by mGluR5 activation and regulates spine morphology. *Curr Biol* 15:587–593.
- Fujimori K, Ishikawa M, Otomo A, Atsuta N, Nakamura R, Akiyama T, Hadano S, Aoki M, Saya H, Sobue G, Okano H (2018) Modeling sporadic ALS in iPSC-derived motor neurons identifies a potential therapeutic agent. *Nat Med* 24:1579–1589.
- Garone MG, Alfano V, Salvatori B, Braccia C, Peruzzi G, Colantoni A, Bozzoni I, Armirotti A, Rosa A (2020) Proteomics analysis of FUS mutant human motoneurons reveals altered regulation of cytoskeleton and other ALS-linked proteins via 3'UTR binding. *Sci Rep* 10:11827.
- Groen EJ, Fumoto K, Blokhuis AM, Engelen-Lee J, Zhou Y, van den Heuvel DM, Koppers M, van Diggelen F, van Heest J, Demmers JA, Kirby J, Shaw PJ, Aronica E, Spliet WG, Veldink JH, van den Berg LH, Pasterkamp RJ (2013) ALS-associated mutations in FUS disrupt the axonal distribution and function of SMN. *Hum Mol Genet* 22:3690–3704.
- Hayashi N, et al. (2020) Prognosis of amyotrophic lateral sclerosis patients undergoing tracheostomy invasive ventilation therapy in Japan. *J Neurol Neurosurg Psychiatry* 91:285–290.
- Henstridge CM, Sideris DI, Carroll E, Rotariu S, Salomonsson S, Tziaras M, McKenzie C-A, Smith C, von Arnim CAF, Ludolph AC, Lulé D, Leighton D, Warner J, Cleary E, Newton J, Swingler R, Chandran S, Gillingwater TH, Abrahams S, Spires-Jones TL (2018) Synapse loss in the prefrontal cortex is associated with cognitive decline in amyotrophic lateral sclerosis. *Acta Neuropathol* 135:213–226.
- Hermis J, Dorostkar MM (2016) Dendritic spine pathology in neurodegenerative diseases. *Annu Rev Pathol* 11:221–250.
- Hofweber M, Hutten S, Bourgeois B, Spreitzer E, Niedner-Boblenz A, Schifferer M, Ruepp MD, Simons M, Niessing D, Madl T, Dormann D (2018) Phase separation of FUS is suppressed by its nuclear import receptor and arginine methylation. *Cell* 173:706–719.e13.
- Humphrey J, et al. (2020) FUS ALS-causative mutations impair FUS autoregulation and splicing factor networks through intron retention. *Nucleic Acids Res* 48:6889–6905.
- Imamura K, et al. (2017) The Src/c-Abl pathway is a potential therapeutic target in amyotrophic lateral sclerosis. *Sci Transl Med* 9:eaaf3962.
- Ishigaki S, Sobue G (2018) Importance of functional loss of FUS in FTLD/ALS. *Front Mol Biosci* 5:44.
- Ishigaki S, Masuda A, Fujioka Y, Iguchi Y, Katsuno M, Shibata A, Urano F, Sobue G, Ohno K (2012) Position-dependent FUS-RNA interactions regulate alternative splicing events and transcriptions. *Sci Rep* 2:529.
- Jeyabalan N, Clement JP (2016) *SYNGAP1*: mind the Gap. *Front Cell Neurosci* 10:32.
- Kamelgarn M, Chen J, Kuang L, Jin H, Kasarskis EJ, Zhu H (2018) ALS mutations of FUS suppress protein translation and disrupt the regulation of nonsense-mediated decay. *Proc Natl Acad Sci USA* 115:E11904–E11913.
- Kapeli K, et al. (2016) Distinct and shared functions of ALS-associated proteins TDP-43, FUS and TAF15 revealed by multisystem analyses. *Nat Commun* 7:12143.
- Karczewski KJ, et al. (2020) The mutational constraint spectrum quantified from variation in 141,456 humans. *Nature* 581:434–443.
- Kilinc M, Creson T, Rojas C, Aceti M, Ellegood J, Vaissiere T, Lerch JP, Rumbaugh G (2018) Species-conserved *SYNGAP1* phenotypes associated with neurodevelopmental disorders. *Mol Cell Neurosci* 91:140–150.
- Kim JH, Liao D, Lau LF, Haganir RL (1998) SynGAP: a synaptic RasGAP that associates with the PSD-95/SAP90 protein family. *Neuron* 20:683–691.
- Kim JH, Lee HK, Takamiya K, Haganir RL (2003) The role of synaptic GTPase-activating protein in neuronal development and synaptic plasticity. *J Neurosci* 23:1119–1124.
- Kole R, Krainer AR, Altman S (2012) RNA therapeutics: beyond RNA interference and antisense oligonucleotides. *Nat Rev Drug Discov* 11:125–140.
- Kwiatkowski TJ Jr, et al. (2009) Mutations in the FUS/TLS gene on chromosome 16 cause familial amyotrophic lateral sclerosis. *Science* 323:1205–1208.
- Lagier-Tourenne C, et al. (2012) Divergent roles of ALS-linked proteins FUS/TLS and TDP-43 intersect in processing long pre-mRNAs. *Nat Neurosci* 15:1488–1497.
- Liepert A, Mossanen JC, Denecke B, Heymann F, De Santis R, Tacke F, Marx G, Ostareck DH, Ostareck-Lederer A (2014) Translation control of

- TAK1 mRNA by hnRNP K modulates LPS-induced macrophage activation. *RNA* 20:899–911.
- Liu L, Luo C, Luo Y, Chen L, Liu Y, Wang Y, Han J, Zhang Y, Wei N, Xie Z, Wu W, Wu G, Feng Y (2018) MRPL33 and its splicing regulator hnRNPK are required for mitochondria function and implicated in tumor progression. *Oncogene* 37:86–94.
- López-Erauskin J, et al. (2018) ALS/FTD-linked mutation in FUS suppresses intra-axonal protein synthesis and drives disease without nuclear loss-of-function of FUS. *Neuron* 100:816–830.e7.
- Mackenzie IR, Ansorge O, Strong M, Bilbao J, Zinman L, Ang LC, Baker M, Stewart H, Eisen A, Rademakers R, Neumann M (2011) Pathological heterogeneity in amyotrophic lateral sclerosis with FUS mutations: two distinct patterns correlating with disease severity and mutation. *Acta Neuropathol* 122:87–98.
- Marchand V, Santerre M, Aigueperse C, Fouillen L, Saliou JM, Van Dorsselaer A, Sanglier-Cianféran S, Branlant C, Motorin Y (2011) Identification of protein partners of the human immunodeficiency virus 1 tat/rev exon 3 leads to the discovery of a new HIV-1 splicing regulator, protein hnRNP K. *RNA Biol* 8:325–342.
- Masuda A, Takeda J, Okuno T, Okamoto T, Ohkawara B, Ito M, Ishigaki S, Sobue G, Ohno K (2015) Position-specific binding of FUS to nascent RNA regulates mRNA length. *Genes Dev* 29:1045–1057.
- McMahon AC, Barnett MW, O’Leary TS, Stoney PN, Collins MO, Papadia S, Choudhary JS, Komiyama NH, Grant SG, Hardingham GE, Wyllie DJ, Kind PC (2012) SynGAP isoforms exert opposing effects on synaptic strength. *Nat Commun* 3:900.
- Michelotti EF, Michelotti GA, Aronsohn AI, Levens D (1996) Heterogeneous nuclear ribonucleoprotein K is a transcription factor. *Mol Cell Biol* 16:2350–2360.
- Mignot C, et al. (2016) Genetic and neurodevelopmental spectrum of SYNGAP1-associated intellectual disability and epilepsy. *J Med Genet* 53:511–522.
- Nakamura R, et al. (2021) Genetic and functional analysis of KIF5A variants in Japanese patients with sporadic amyotrophic lateral sclerosis. *Neurobiol Aging* 97:147.e11–147.e17.
- Nakaya T, Alexiou P, Maragkakis M, Chang A, Mourelatos Z (2013) FUS regulates genes coding for RNA-binding proteins in neurons by binding to their highly conserved introns. *RNA* 19:498–509.
- Neumann M, Rademakers R, Roeber S, Baker M, Kretschmar HA, Mackenzie IR (2009) A new subtype of frontotemporal lobar degeneration with FUS pathology. *Brain* 132:2922–2931.
- Niaki AG, Sarkar J, Cai X, Rhine K, Vidaurre V, Guy B, Hurst M, Lee JC, Koh HR, Guo L, Fare CM, Shorter J, Myong S (2020) Loss of dynamic RNA interaction and aberrant phase separation induced by two distinct types of ALS/FTD-linked FUS mutations. *Mol Cell* 77:82–94.e4.
- Odawara A, Katoh H, Matsuda N, Suzuki I (2016) Physiological maturation and drug responses of human induced pluripotent stem cell-derived cortical neuronal networks in long-term culture. *Sci Rep* 6:26181.
- Okada R, Onodera K, Ito T, Doyu M, Okano HJ, Okada Y (2021) Modulation of oxygen tension, acidosis, and cell density is crucial for neural differentiation of human induced pluripotent stem cells. *Neurosci Res* 163:34–42.
- Onodera K, Shimojo D, Ishihara Y, Yano M, Miya F, Banno H, Kuzumaki N, Ito T, Okada R, de Araújo Herculano B, Ohyama M, Yoshida M, Tsunoda T, Katsuno M, Doyu M, Sobue G, Okano H, Okada Y (2020) Unveiling synapse pathology in spinal bulbar muscular atrophy by genome-wide transcriptome analysis of purified motor neurons derived from disease specific iPSCs. *Mol Brain* 13:18.
- Popovitchenko T, et al. (2020) Translational derepression of Elavl4 isoforms at their alternative 5’ UTRs determines neuronal development. *Nat Commun* 11:1674.
- Qiu H, Lee S, Shang Y, Wang WY, Au KF, Kamiya S, Barmada SJ, Finkbeiner S, Lui H, Carlton CE, Tang AA, Oldham MC, Wang H, Shorter J, Filiano AJ, Roberson ED, Tourtellotte WG, Chen B, Tsai LH, Huang EJ (2014) ALS-associated mutation FUS-R521C causes DNA damage and RNA splicing defects. *J Clin Invest* 124:981–999.
- Rumbaugh G, Adams JP, Kim JH, Hagan RL (2006) SynGAP regulates synaptic strength and mitogen-activated protein kinases in cultured neurons. *Proc Natl Acad Sci U S A* 103:4344–4351.
- Sasaki S, Maruyama S (1994) Synapse loss in anterior horn neurons in amyotrophic lateral sclerosis. *Acta Neuropathol* 88:222–227.
- Sharma A, Lyashchenko AK, Lu L, Nasrabad SE, Elmaleh M, Mendelsohn M, Nemes A, Tapia JC, Mentis GZ, Shneider NA (2016) ALS-associated mutant FUS induces selective motor neuron degeneration through toxic gain of function. *Nat Commun* 7:10465.
- Shimojo D, Onodera K, Doi-Torii Y, Ishihara Y, Hattori C, Miwa Y, Tanaka S, Okada R, Ohyama M, Shoji M, Nakanishi A, Doyu M, Okano H, Okada Y (2015) Rapid, efficient, and simple motor neuron differentiation from human pluripotent stem cells. *Mol Brain* 8:79.
- Shin CH, Lee H, Kim HR, Choi KH, Joung JG, Kim HH (2017) Regulation of PLK1 through competition between hnRNPK, miR-149-3p and miR-193b-5p. *Cell Death Differ* 24:1861–1871.
- Sunico CR, Domínguez G, García-Verdugo JM, Osta R, Montero F, Moreno-López B (2011) Reduction in the motoneuron inhibitory/excitatory synaptic ratio in an early-symptomatic mouse model of amyotrophic lateral sclerosis. *Brain Pathol* 21:1–15.
- Tadaka S, Saigusa D, Motoike IN, Inoue J, Aoki Y, Shirota M, Koshiba S, Yamamoto M, Kinoshita K (2018) jMorp: Japanese multi omics reference panel. *Nucleic Acids Res* 46:D551–D557.
- Takahashi K, Tanabe K, Ohnuki M, Narita M, Ichisaka T, Tomoda K, Yamanaka S (2007) Induction of pluripotent stem cells from adult human fibroblasts by defined factors. *Cell* 131:861–872.
- Takayama K, Igai K, Hagihara Y, Hashimoto R, Hanawa M, Sakuma T, Tachibana M, Sakurai F, Yamamoto T, Mizuguchi H (2017) Highly efficient biallelic genome editing of human ES/iPS cells using a CRISPR/Cas9 or TALEN system. *Nucleic Acids Res* 45:5198–5207.
- Tan AY, Manley JL (2010) TLS inhibits RNA polymerase III transcription. *Mol Cell Biol* 30:186–196.
- Thompson MG, Muñoz-Moreno R, Bhat P, Roytenberg R, Lindberg J, Gazzara MR, Mallory MJ, Zhang K, Garcia-Sastre A, Fontoura BMA, Lynch KW (2018) Co-regulatory activity of hnRNP K and NS1-BP in influenza and human mRNA splicing. *Nat Commun* 9:2407.
- Udagawa T, Fujioka Y, Tanaka M, Honda D, Yokoi S, Riku Y, Ibi D, Nagai T, Yamada K, Watanabe H, Katsuno M, Inada T, Ohno K, Sokabe M, Okado H, Ishigaki S, Sobue G (2015) FUS regulates AMPA receptor function and FTL/ALS-associated behaviour via GluA1 mRNA stabilization. *Nat Commun* 6:7098.
- Vuong JK, Ergin V, Chen L, Zheng S (2022) Multilayered regulations of alternative splicing, NMD, and protein stability control temporal induction and tissue-specific expression of TRIM46 during axon formation. *Nat Commun* 13:2081.
- Walkup WG, Mastro TL, Schenker LT, Vielmetter J, Hu R, Iancu A, Reghunathan M, Bannon BD, Kennedy MB (2016) A model for regulation by SynGAP- $\alpha$ 1 of binding of synaptic proteins to PDZ-domain ‘Slots’ in the postsynaptic density. *Elife* 5:e16813.
- Wang Z, Qiu H, He J, Liu L, Xue W, Fox A, Tickner J, Xu J (2020) The emerging roles of hnRNPK. *J Cell Physiol* 235:1995–2008.
- Yano M, Okano HJ, Okano H (2005) Involvement of Hu and heterogeneous nuclear ribonucleoprotein K in neuronal differentiation through p21 mRNA post-transcriptional regulation. *J Biol Chem* 280:12690–12699.
- Yasuda K, Zhang H, Loiselle D, Haystead T, Macara IG, Mili S (2013) The RNA-binding protein Fus directs translation of localized mRNAs in APC-RNP granules. *J Cell Biol* 203:737–746.
- Yokoi S, Udagawa T, Fujioka Y, Honda D, Okado H, Watanabe H, Katsuno M, Ishigaki S, Sobue G (2017) 3’UTR length-dependent control of SynGAP isoform  $\alpha$ 2 mRNA by FUS and ELAV-like proteins promotes dendritic spine maturation and cognitive function. *Cell Rep* 20:3071–3084.
- Yoshimatsu S, Sone T, Nakajima M, Sato T, Okochi R, Ishikawa M, Nakamura M, Sasaki E, Shiozawa S, Okano H (2019) A versatile toolbox for knock-in gene targeting based on the multisite gateway technology. *PLoS One* 14:e0221164.
- Zhao X, Zhu D, Zhang H, Sui H, Poon V, Jiang S, Zheng B (2019) A natural “GA” insertion mutation in the sequence encoding the 3’UTR of CXCL12/SDF-1 $\alpha$ : identification, characterization, and functional impact on mRNA splicing. *Gene* 681:36–44.